의학박사 학위논문

Dynamic change of hierarchical core voxels of functional brain network in aging

노화에서 뇌기능신경망으로부터 추출한 코어복셀 위계구조의 역동적 변화

2023년 2월

서울대학교 융합과학기술대학원

분자의학 및 바이오제약학과

김 현 주

Dynamic change of hierarchical core voxels of functional brain network in aging

지도 교수 이 동 수

이 논문을 의학박사 학위논문으로 제출함

2023년 2월

서울대학교 융합과학기술대학원

분자의학 및 바이오제약학과

김 현 주

김현주의 의학박사 학위논문을 인준함

2023년 2월

위 원 장 이 재 성 (인)

부위원장 이 동 수 (인)

위 원 신 영 기 (인)

위 원 강 혜 진 (인)

위 원 하 승 균 (인)

Abstract

Dynamic change of hierarchical core voxels of functional brain network in aging

Hyun Joo Kim

Department of Molecular Medicine and Biopharmaceutical Science,

The Graduate School of Convergence Science and Technology

Seoul National University

Many methods were developed to assess the functional intervoxel connectivity to discover and better understand the brain function in individuals. In this study, k-core percolation method was assessed to reveal the dynamic hierarchical structure on resting-state fMRI (rsfMRI) on voxel-level and the feasibility of the method was evaluated by applying it in the aging process.

Total 70 individuals were included in this study, 32 individuals from Alzheimer's Disease Neuroimaging Initiative (ADNI) and 38 individuals from Seoul National University (SNU). K-core percolation method, a voxel-based approach was applied to reveal the hierarchical structure of voxels in the brain. k_{max}-core and coreness k values derived from k-core percolation characterizing the time-varying core voxels were visualized on various plots to visualize the dynamic hierarchical structure more intuitively. Independent component analysis (ICA)

was carried out to label the associated functional independent components (IC) of the identified voxel. Analysis was done in both static and dynamic studies, and in positive and negative correlations. Coreness k value map overlaid on brain T1 MRI was generated for further evaluation of the distribution of coreness k values.

Dynamic hierarchical structure of voxels visualized on various plots revealed time-varying change of k_{max}-core voxels and coreness k values, reflecting the dynamic change of brain function in an individual, which was not fully reflected on static functional connectivity. Dynamic flow pattern was different in positive and negative correlations, portraying the dynamic brain function in different neuronal networks. Coreness k value map revealed altered distribution of coreness k values in the brain. Asymmetric, unsynchronized distribution was deteriorated in the aging process. This asymmetry detected on dynamic coreness k map was assessed quantitatively by measuring asymmetry index, which revealed distinctive difference between young and aged healthy control group. The difference was more evident on dynamic study than static study. Also, as the age increased, coreness k values from static and dynamic studies decreased in all IC regions, which represents decreased connectivity in aging.

Investigation of dynamic functional connectivity with k-core percolation on voxel-level revealed dynamic hierarchical structure of voxels, reflecting the time-varying brain function in individuals. Dynamic functional connectivity is more appropriate to investigate one's brain function, since it contains the time-varying information which is not well reflected on static functional connectivity. With this method, characteristics of dynamic hierarchical structure of an

individual can be discovered and have shown possibility of further clinical application.

Keywords : dynamic functional connectivity, k-core percolation, hierarchical structure, resting-state fMRI, aging

Student Number : 2015-26074

Table of Contents

List of Tables

List of Figures

List of Supplementary Figures and Movies

INTRODUCTION

Dynamic functional brain connectivity in rsfMRI

Resting-state functional MRI (rsfMRI) is an imaging method used to assess the regional interaction or connectivity within the brain, which seems to change dynamically over time. Brain connectivity on rsfMRI is assessed with blood-oxygen-level dependent (BOLD) signals, which reflects the change of blood flow in the brain (1). Though not fully understood, researchers assume that the BOLD signals from rsfMRI reflect the brain function during the entire acquisition time or at the certain time bins (2). The former is called static study and the latter is dynamic study of functional brain connectivity on rsfMRI (3, 4, 5, 6, 7, 8, 9, 10, 11). Conventionally, functional connectivity in rsfMRI has been assessed as the static study, neglecting the implicit time-varying information. To accommodate the temporal information in the analysis, various method to materialize dynamic study has been investigated. Most common method for dynamic study in fMRI is the sliding window analysis, by dividing the entire time course into a sequence of sliding windows and measuring functional connectivity in each window (12). Sliding window method is characterized by selecting certain time window, and this window is shifted in time by a fixed number of data points, called step, defining the overlap between two successive windows (13).

To extract functional connectivity patterns with temporal information, several methods have been developed, such as model-based or seeds-based brain-search methods. Hidden Markov model (HMM) is a model-based approach, which

generate time-varying states of a few clusters of spatial principal components using brain voxels (14, 15, 16, 17, 18). In HMM, individual rsfMRI volumes are modeled as a mixture of the brain states and linked to each state with a given probability. In HMM, the functional connectivity is only displayed as switches between states, so choosing the adequate state was essential (2). Also, the analysis was performed in a few to dozen state units, which was composed of thousands of voxels (18). The seeds-based approach is called co-activation pattern (CAP) of searched voxels and the seeds are composed of voxels of interest (VOI), which is made up of thousands of voxels, as well (19, 20, 21). A subset of time points was divided by clustering algorithm that show high activity at a specific seed region into multiple subgroups based on their spatial similarity, and then the volumes were averaged within each subgroup to generate CAPs. Despite the efforts to assess the dynamic functional connectivity, both approaches have potential computational problem and choosing the optimal output states in HMM or seeds in CAP approaches is another drawback for further analysis on individuals' dynamic brain functions. Furthermore, these analytic methods are based on units of states or seeds, which are composed of thousands of voxels. Composition of thousands of voxels lead to the problem of heterogeneity of the unit itself. So further breakdown of units into much smaller number of voxels is necessary to overcome the heterogeneity.

Functional brain networks have the characteristics of an open disperse system (22) with metastability (23, 24, 25) resulting in the state progressions with intermittent transition (26), whose underlying mechanism lies in intrinsic composition of network nodes. These network nodes or voxels are considered as

the units of brain function, and a voxel in current mm^3 resolution of fMRI contain cluster of 10^5 neurons (27). So, the voxel itself can still be heterogeneous and stationarity within the time bins are unproven, but analysis on voxel-level assuming stationarity within the voxel is worthwhile, overcoming the previous limitations in dynamic functional connectivity analyses (9, 10, 28, 29).

k-core percolation

A method called *k*-core percolation has been recently introduced (30, 31). *k*-core percolation investigates individual-specific core subnetworks of brain connectivity. It is voxel-based approach, which displays functional hierarchical structure of every voxel on recursive analysis. *k*-core is identified by pruning all voxels with degree lower than *k* until no remaining voxel with a degree less than k is left. k_{max}-core voxels at the uppermost hierarchy are considered the most influential nodes at that moment. A sliding window method, using 1-min time bins of 2 seconds shift for individuals, was used to produce the consecutive 116 or 93 bins per subject, to analyze on dynamic basis. According to this analysis, the state progress and transition of voxels representing hierarchical structures were found to be diverse with various compositions of functional independent components (ICs) (32). This voxel-based approach led to implement various visualization methods, which are coreness *k* flag plots, bar plots, k_{max}-core stacked histogram, coreness *k* map.

Functional intervoxel connectivity on rsfMRI was transformed to coreness *k* values for voxels, using node (voxel) instead of edge (correlation or connectivity)

information for visualization, and hierarchical intervoxel connectivity was interpreted in the voxel-level. Further evaluation was performed with intervoxel negative correlation to produce the negative-influence networks and absolute values from negative correlation were used for analysis. Also, positive and negative correlations were combined together to assess both influencing networks.

Various plots were generated with coreness k or k_{max}-core voxels to display functional intervoxel connectivity, using positive correlation and negative correlation after thresholding to confirm the scale-freeness. It was applied in individuals from Alzheimer's Disease Neuroimaging Initiative (ADNI) and our institution (SNU), on the static (10 minutes or 7 minutes, respectively for ADNI or SNU) and the dynamic (116 1-min-bins with 2-sec shifts (ADNI) or 93 1-min-bins with 2-sec shifts (SNU)) studies. On the dynamic study, change of k_{max}-core composition and state transition over time were assessed, and these were classified into designated IC-maps, to determine the most influential IC at that moment. These figures and animations were generated to facilitate the interpretation of dynamic hierarchical structure of an individual's brain function on voxel-level, anticipating further application in clinical settings as well. In this study, this k-core percolation method was applied in young and aged normal cognitive group to evaluate the feasibility of the method in assessing aging process.

Functional connectivity in aging process

Various imaging modalities have been investigated in the aging to unveil the underlying mechanism in the aging process. MRI has been investigated to find the structural abnormality associated with neurodegeneration. PET imaging with various types of tracers such as FDG, amyloid-β, tau have been used to assess change in the glucose metabolism or accumulation of amyloid or tau proteins in aging or senile neurodegenerative diseases (33, 34).

Functional brain connectivity has been emerged as an important biomarker for understanding aging and neurodegenerative diseases (35, 36, 37, 38, 39, 40, 41). fMRI has emerged as an imaging tool to measure the altered brain connectivity and dysfunction indirectly. The spontaneous low-frequency (<0.001–0.100 Hz) fluctuations of the BOLD signals can be measured from rsfMRI, and the correlations from the BOLD signals are generated into adjacency matrices to find the most affected region in the brain (35, 41). While previous studies have focused on revealing functional connectivity in brain regions on static fMRI, nowadays dynamic functional connectivity assessment is performed with BOLD signals (6, 10, 41), which is applied in the investigation of aging and neurodegenerations.

Some features have been detected in previous functional connectivity studies of aging. One feature is the reduced connectivity (38, 42). Brain network is affected by aging, resulting in decreased connectivity within the networks such as primary sensory and cognitive networks. Several studies have suggested default mode

network (DMN) as the major hub for functional brain connectivity in aging. Along with aging, decreased connectivity in DMN has been observed most frequently in the neurodegenerative diseases as well, which was also correlated with severity of cognitive decline (35, 43, 44, 45, 46). Other networks such as dorsal attention network (DAN), salience network (SN) and sensorimotor network (SMN) have also been identified to contribute or be sensitive in aging (42).

Another feature in the aging brain is asymmetry (47, 48). There are still controversies with mixed results in asymmetry observed in the aging brain, but it is quite evident that asymmetry plays some role in aging process. Left and right asymmetry in the insula regions increasing with age was observed (48). Altered cortical activation pattern called poster-anterior shift in aging (PASA) was observed in the aged population, which is referring to tendency of decreased activity in occipitotemporal regions and increased activity in the prefrontal cortex, suggesting neural activation shifting from the posterior (sensory) to the anterior (cognition) areas. Also, there is a phenomenon called hemispheric asymmetry reduction in older adults (HAROLD) reported in aging (49, 50). This is characterized by reduced asymmetry in the bilateral hemisphere by reorganization of brain connectivity resulting in increased activation in the previously low activity region, compensating for decreased unilateral neural efficiency, which in turn leads to rather decreased asymmetry in the aged population.

PURPOSE

The purpose of this study was to reveal the dynamic hierarchical structure on voxel-level with k-core percolation method. Unveiled dynamic hierarchical structure was plotted on various figures and animations for more simple and intuitive interpretations. k-core percolation method was implemented to generate dynamic and static functional connectivity and these studies were compared to define the characteristics of dynamic study from static study. Dynamic functional connectivity was assessed in positive and negative correlations, and these correlations combined as well, and the results were compared. After evaluating the overall integrity of the method, this method was applied in individuals in the aging process to evaluate the feasibility of the method in clinical applications.

MATERIALS AND METHODS

Data preprocessing

rsfMRI data of aged healthy control patients (aged HC, aHC) were downloaded from the ADNI (https://adni.loni.usc.edu/data-samples/access-data/). Total 32 participants were included, aged from 65 to 95 without any significant history of psychiatric disorder, neurological or cardiovascular disease (Table 1). Minimally preprocessed rsfMRI data were used (51) and further preprocessing was performed: smoothing using 6 mm full-width at half maximum of Gaussian kernel, bandpass filtering (0.01 Hz – 0.1 Hz). Next, the data were downsampled to 31 x 37 x 31 dimension with 6 x 6 x 6 mm^3 size-voxel to reduce computational load. A mask was applied to exclude voxels that do not belong to the gray matter, finally including in 5,937 voxels for the analysis.

Additionally, rsfMRI data of normal individuals were retrieved from our institution (SNU)'s database as well, to represent normal individual (young HC, yHC). 38 normal patients aged from 21 to 71 without any significant history of psychiatric disorder, neurological or cardiovascular disease were included. rsfMRI data were preprocessed using smoothing with 6mm full-width at half maximum of Gaussian kernel, bandpass filtering (0.01 Hz – 0.1 Hz). The temporal filtering with 0.01 to 0.1 Hz and the downsampling were applied as the ADNI data, and total 5,937 voxels were included for analysis with 6 x 6 x 6 mm^3.

Table 1. Demographics of study subjects

	SNU	ADNI
Number	38	32
Age	43.9 ± 14.0 (21 – 71)	75.7 ± 7.0 (65 – 95)
Sex (M:F)	19:19	11:21
MMSE	29.4 ± 0.9	29.2 ± 1.3

Table 2. Thresholds of groups

	Static				Dynamic			
	Positive	% of node	Negative	% of node	Positive	% of node	Negative	% of node
SNU	0.55	95.2	0.55	91.2	0.85	94.1	0.80	95.3
ADNI	0.60	92.6	0.45	90.6	0.80	87.0	0.75	94.6

Spatial information from independent component analysis

Spatial information from independent component analysis (ICA) was applied as regional brain atlas to find ICs of the resting-state networks, which was previously retrieved using Multivariate Exploratory Linear Decomposition into Independent Components (MELODIC) (32). Spatial IC maps were applied, and threshold ($Z > 6$) were applied to generate binary masks. In the previous study (31), 15 ICs were included: aDMN (anterior default mode network), DMN, PCN (precuneus network, equivalent to posterior DMN), SN (salience network), DAN (dorsal attention network), L CEN (left central executive network), R CEN (right CEN), SMN (sensorimotor network) 1, SMN2, AN (auditory network), VN (visual network) 1, VN2, VN3, VN4, and VAN (ventral attention network). These 15 ICs were classified into seven categories for comprehensibility: DMN, SN, DAN, CEN, SMN, AN, and VN and the remaining unclassified regions as UNC (unclassified network) (Fig. S1).

Sliding-window analysis

rsfMRI data retrieved from ADNI and SNU were analyzed (Table 1). Sliding-window analysis was used to investigate the nonstationary and time-varying dynamics of the brain connectivity. For ADNI data, the window size was set close to 1 minute (20 volumes, 60 sec) with a shift of 2 sec, resulting in 116 windows. A connectivity matrix of each window was constructed to conduct k-core percolation. To find the ideal threshold determining inverse linearity on the log-log plots, these matrices were displayed for degree distribution to confirm the

scale-freeness of degree distribution, and average 93.9% of the entire voxels were included after thresholding (52). Thresholds varied among the groups, in static and dynamic studies, and in positive and negative correlations (Table 2). After applying the ideal threshold, adjacency matrices made with these thresholds were put into *k*-core percolation (30, 53), which produced 5,937 x 116 percolated matrix for coreness *k* values. Edges with values greater than the threshold were assigned as 1 and otherwise 0. These coreness *k* values of each voxel were rearranged according to the classified ICs (Fig. S1) (DMN, SN, DAN, CEN, SMN, AN, VN, UNC) shown as 116 flag plots on animation in ADNI data.

For CN-SNU normal data, window size was set to 1 minute (20 volumes) with a shift of 3.5 sec. *k*-core percolation was calculated from the connectivity matrix of each window and binary matrix was generated in the same way as ADNI data, producing 5,937 x 93 percolated matrix for coreness *k* values. Edges with values greater than the threshold were assigned as 1 and otherwise 0 to make adjacency matrix. With these thresholds, more than 93.2% of the voxels were included in the study.

From the CN-SNU data, healthy control subjects with age over 60 years old, which was six subjects, were included in the aged healthy control (aHC) for the analysis. The rest 32 subjects with age younger than 60 years old were classified as young healthy control (yHC).

Appliciation of k-core percolation

k-core percolation was carried out to investigate the hierarchical core structure

of a functional brain network using the voxel (node) as the analytic unit (23, 25, 30). This procedure first removes nodes of degree 1 (k = 1). As the nodes are removed, the degree of the remaining nodes is also changed. Nodes, whose degrees are higher, are eventually removed if they meet the removal criteria while k increases. The procedure is performed recursively by incrementing k by 1 until no further process is possible. A subgraph, called k-core, is obtained when all nodes with degree less than k is removed. The last surviving core is called k_{max}-core, and it is considered the voxel with the highest hierarchy, the most influential voxel, which change spontaneously at rest during acquisition period. After conducting k-core percolation, k_{max}-core voxels are categorized into functional ICs determined by group ICA, to identify the uppermost IC subnetworks contributing to the mental state at the precise moment. All the voxels are given the k values of the step when they are removed, and this is called the coreness k value of each voxel.

For dynamic study, 116 time-bins of ADNI individuals and 93 time-bins of SNU individuals were put into the k-core percolation. The coreness k values were used for making animated flag plots, coreness k value map, and IC-based k_{max}-core voxel compositions were used for making stacked histogram, brain-rendered k_{max}-core images.

Coreness k value map

To visualize the coreness k value more intuitively, 6x6 multislice coreness k value map was rendered by merging 36 transaxial images of coreness k value

overlaid on brain T1 MRI in rainbow colors, both in static and dynamic studies. For the dynamic studies, these coreness k value map images of all windows (116 or 93 windows) were merged in animated format to visualize the time-varying change of coreness k value on brain. For the scale of the color bar, a value of 95% of individual k_{max} was set.

Summation of dynamic coreness k values

Coreness k values from the whole acquired time constituting the dynamic study were summed to compare with the coreness k values from the static study. Summed dynamic coreness k values were laid out on a 6x6 multislice coreness k map to compare with static coreness k map. Also, the coreness k values from both positive and negative correlations were summed to include both correlated networks and it was compared between dynamic and static studies. Similarities between the studies were assessed visually and quantitatively with correlation plots.

Quantitative Analysis of Asymmetry Index

Asymmetry index was used to evaluate the asymmetric distribution of coreness k values detected on dynamic coreness k map. Asymmetry index was measured by dividing the brain regions into left and right, anatomically (11 brain regions) or functionally (7 IC regions). Asymmetry indexes were applied both in static and dynamic studies with coreness k values summed from positive and negative correlations. The results were compared between young and aged normal groups.

To assess the time-varying change of asymmetry index of a subject in the dynamic studies, variance of asymmetry index was measured to assess the temporal change of asymmetry index.

Voxel-based Analysis of coreness k values

Voxel-based analysis was done with coreness *k* values of 5937 voxels. These coreness *k* values of static and dynamic studies were classified into 7 IC regions. Mean value of static and dynamic coreness *k* value of each subject was measured and the correlation between the age and coreness *k* values of 7 IC regions were assessed to visualize the change of coreness *k* values upon age.

Statistical analysis was performed to quantitate the comparison between the groups. Non-parametric tests such as Mann Whitney U test, Kruskal-Wallis test were performed to compare between the groups and Wilcoxon sign rank test was performed in static and dynamic studies of the individuals. Correlation and regression were executed to see the relationship between variables. P value of less than 0.05 was considered statistically significant. Statistical analysis was carried out with MedCalc® Statistical Software version 20.123 (MedCalc Software Ltd, Ostend, Belgium; https://www.medcalc.org; 2022).

RESULTS

Generation of dynamic hierarchical structure

Hierarchical structure derived from k-core percolation was visualized with animated flag plots, bar plots, stacked-histograms, brain-rendered images (Fig. 1, Movie S1). Animated flag plots displayed the characteristic time-varying changes of pruning pattern of each IC-based voxels upon percolation. The cross section of each IC-voxels at the end of percolation showed the number of coreness k voxels, and the length of flags represented the depth of hierarchical structures of IC-voxels, with the peak of each flag representing the k_{max}-core voxels of each IC at that moment, which are the voxels with uppermost hierarchy (30). Number of k_{max}-core voxels in each IC at certain time bin was expressed on bar plots. k_{max}-core voxels were plotted on animated stacked histograms with designated IC map colors.

States, state transitions, pulses were assessed visually on animated images, identifying the ICs that these voxels belonged to. State transition was visually defined as an abrupt change in k_{max}-core voxels-IC composition to another composition, and number of transitions ranging from 0 to 14 per individuals was observed. When the same k_{max}-core voxels-IC composition was continued for some time, it was defined as smooth progression. Pulse was defined as the tall spike persistent for one or more bins. Right or left-sidedness of k_{max}-core voxels was not expressed on animated stacked histograms but roughly shown on brain-rendered axial images.

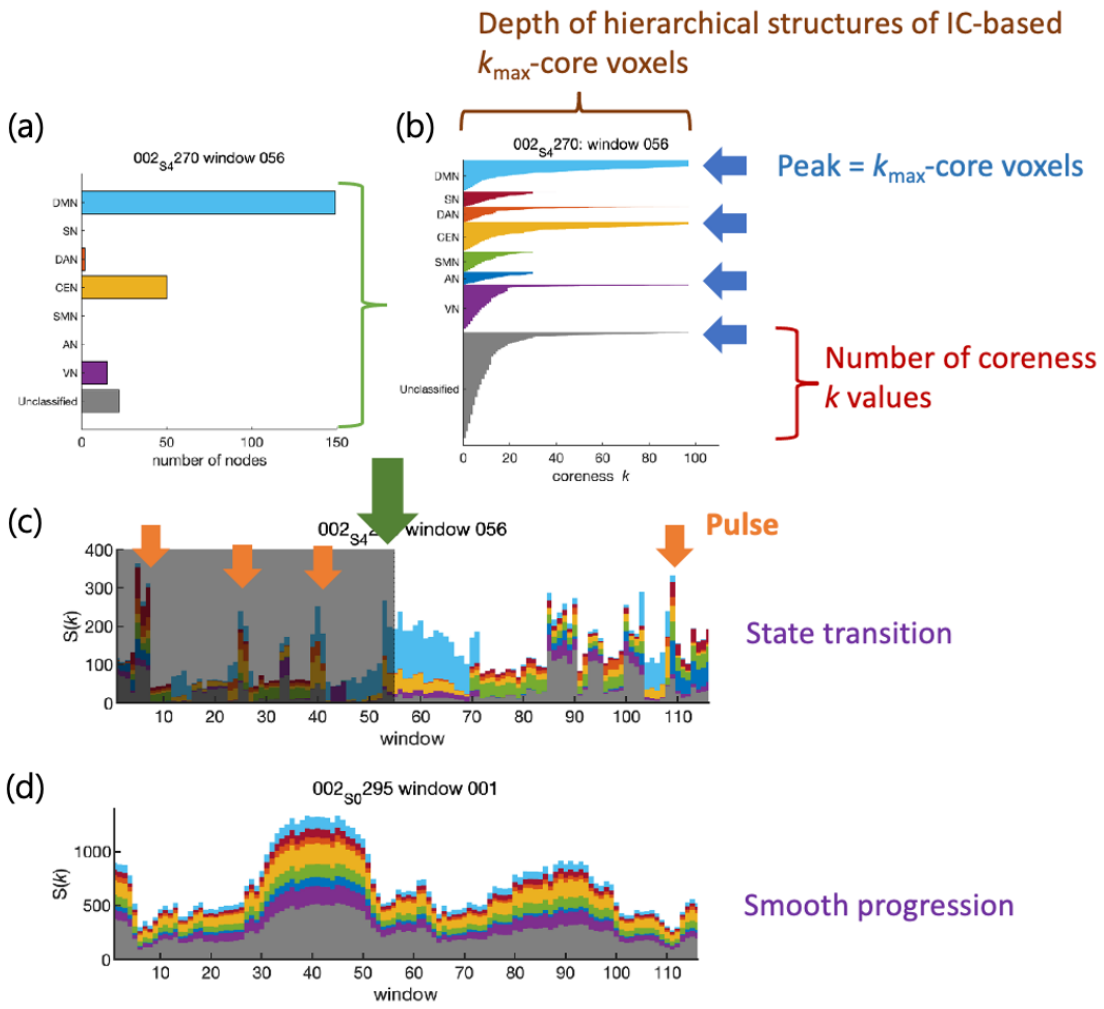

Figure 1. Interpretation of various plots of k_{max}-core voxels and coreness k values. (a) Number of k_{max}-core voxels in each IC at the moment is expressed on bar plots. (b) Depth of hierarchical structures of IC-based k_{max}-core voxels are expressed as length of flag plots and cross section of flag plot mean the number of coreness k voxels. Peak of each flag represent the k_{max}-core voxels of each IC. (c) State transition is abrupt change of k_{max}-core IC-compositions (purple arrows) on the flow pattern and the spikes that appear on the stacked histogram is defined as pulse (orange arrows). (d) Stable, monotonous flow pattern of k_{max}-core IC-composition is defined as smooth progression.

Visual assessment of hierarchical structure in static study

Hierarchical structure revealed by k-core percolation was assessed in both dynamic and static studies. Inter-individual variability of hierarchical structure was noted but these structures were stratified according to the IC-compositions of k_{max}-core voxels, in a similar manner as previous studies (30, 31).

In static study of positive correlations, distributed pattern or IC-dominant patterns of the k_{max}-core voxels (Fig. 2, Fig. S2) was observed. Among 70 individuals regardless of age groups, various types were identified: 19 showed distributed pattern, 4 DMN/CEN, 4 CEN/UNC, 4 VN/SMN, 1 DMN/VN co-dominant types and 3 DMN, 16 VN, 5 SMN-dominant types in positive correlation. 14 showed dominant voxels of UNC.

Static study of negative correlation revealed somewhat different patterns on the IC-composition of the k_{max}-core voxels. Types of patterns were less diverse, rather monotonous than positive correlations. 52 showed distributed pattern, which is about 74% of individuals, 11 with UNC-dominant type, 4 VN, 2 DMN/CEN dominant types and 1 CEN -dominant type.

Regardless of age groups, all individuals showed similar pattern in positive or negative correlations, with diverse types in positive correlation and monotonous distributed or UNC-dominant type in negative correlation.

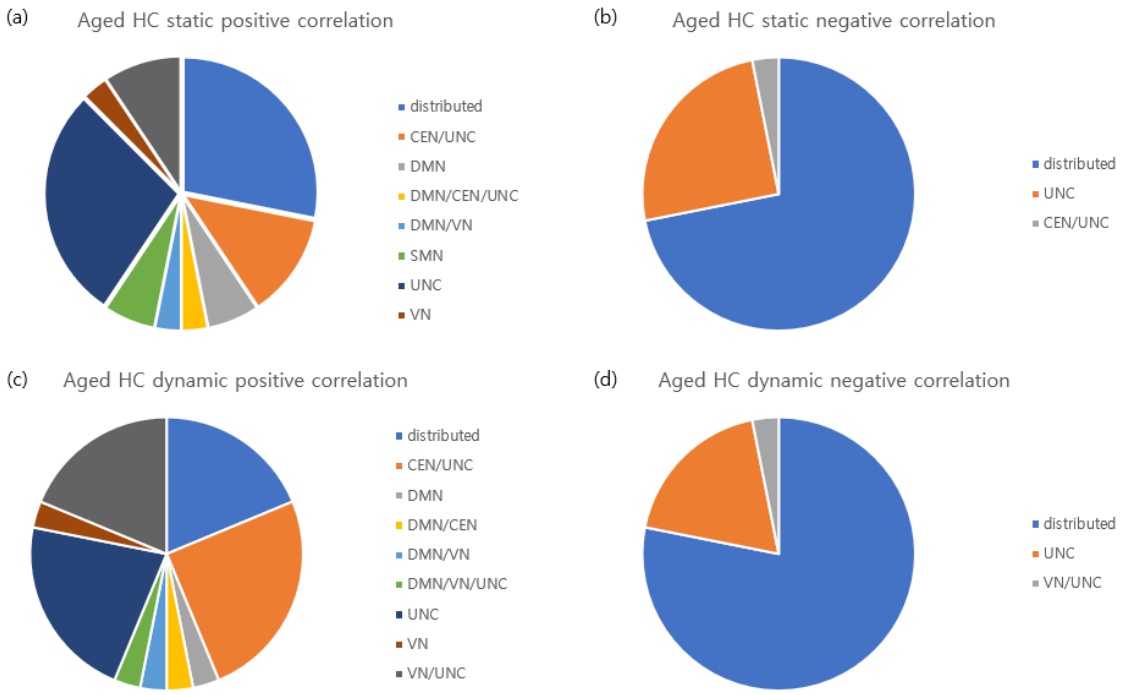

Figure 2. k_{max}-core voxels-IC composition of positive and negative correlations on static and dynamic study in aged HC group. A) On static study of positive correlation, various types were observed with distributed pattern, most prevalent. B) Patterns were less diverse in static negative correlations, with distributed type most predominant. C) On dynamic study of positive correlation, diverse types were observed as static study, with distributed pattern most common. D) As in the static study of negative correlation, patterns were less diverse, with predominant type as the distributed pattern.

Visual assessment of hierarchical structure in dynamic study

Time-varying change of pruning pattern of each IC-based voxels upon k-core percolation was well visualized on animated flag plots. Dynamic change of depth of hierarchical structures of IC-voxels was expressed with the change of flag lengths of each ICs. The temporal change of IC-compositions of k_{max}-core voxels at the uppermost position of k-core percolation were presented as the peaks on animated flag plots and on animated bar plots, stacked histogram and brain-rendered axial images (Fig. 3, Movie. S1).

Proportion of IC-based k_{max}-core voxels were classified with the transition pattern types in the dynamic study. Pulses, states and transition of states were determined visually. Dynamic study of positive correlation revealed diverse pattern of distributed or specific IC-dominant types with time-varying change (Fig. 2, Fig. S2). Concerning k_{max}-core voxels-IC composition, similar tendency was observed as the positive correlation in static study, displaying various pattern types, with distributed type most prevalent. Among 70 individuals, 21 individuals showed distributed pattern, 13 VN-dominant, 8 CEN-dominant, 4 DMN-dominant, 2 DMN/VN co-dominant, 10 UNC-dominant and 1 SMN-dominant type.

State transition, which is an abrupt change in k_{max}-core voxels-IC composition to another composition, was observed with number of transitions ranging from 0 to 14 per individuals. State transitions were observed frequently in positive correlation, without definite directionality. Out of 70 individuals, 63 individuals

exhibited state transitions, with 1 to 14 transitions per individual (Fig. 4A, Movie. S2). State transitions were not predictable, portraying the diversity of an individual's brain function. Pulse, which is defined as the tall spike persistent for one or more bins, was observed with an average number of 5.3 (0 to 17 pulses per individual). Some pulses preceded state transition, but it was not always the case, showing random appearance.

Dynamic study of negative correlation displayed different pattern from positive correlation, and rather displaying similar pattern as the static study of negative correlation (Fig. 2, Fig. S2). 58 individuals, about 83% of individuals showed distributed type in IC-composition patterns. 7 individuals displayed UNC-dominant type and 5 VN/UNC co-dominant types were observed as well. Considerable portion of UNC voxels was observed in significant portion throughout the whole state, all over the cerebral hemisphere and cerebellum.

Unlike positive correlation, abrupt state transitions were less noticed in the negative correlation (Fig. 4B, Movie. S3). About 87% of individuals showed smooth progression over time without significant state transitions. Thus, voxel belonging to certain ICs persisted throughout the entire time bins. Although temporal progression was smooth, pulse was also observed in similar frequency as positive correlation, with about an average number of 5.0 (0 to 16 pulses per individual).

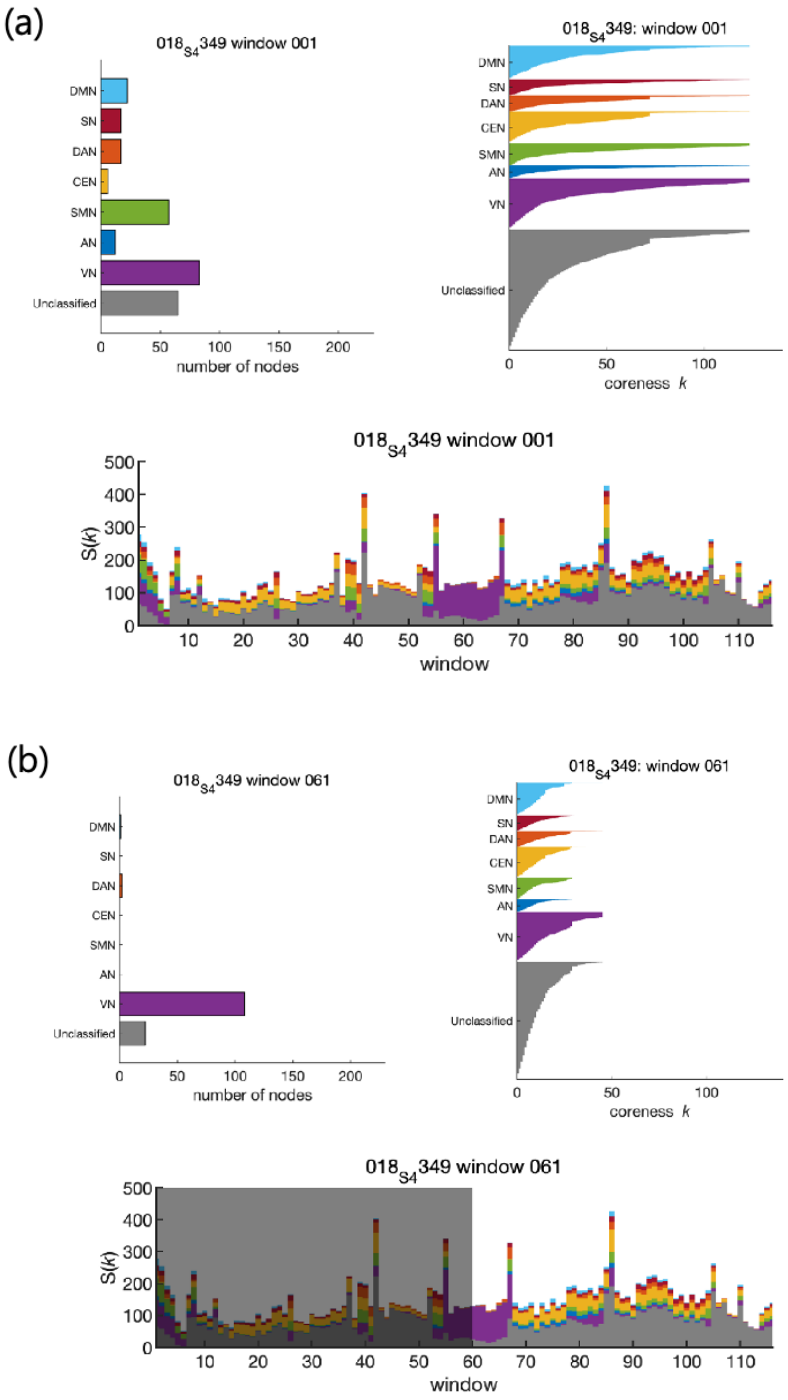

Figure 3. Time-varying change of coreness k value on flag plot and k_{max}-core voxel IC-composition in aged HC subject (F/71.5). Different k_{max}-core voxels IC-compositions are observed along the time. (a) At initial window, various types of IC-voxels are noted on stacked histogram which is reflected on flag plot and bar plot. (b) At window 61, VN-dominant with some UNC-based k_{max}-core voxels are noted on bar plot and peak of flag plot.

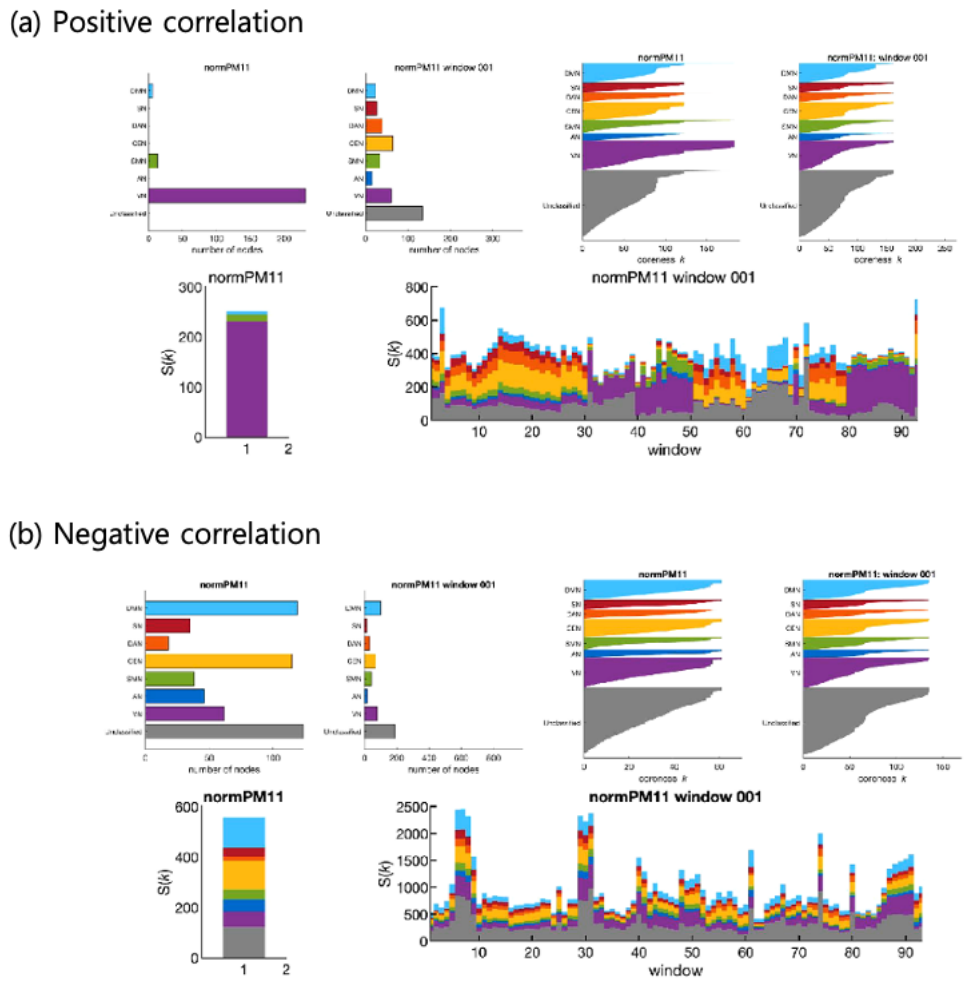

Fig 4. Different pattern of coreness k value and k_{max}-core voxel IC-composition in positive and negative correlation in an individual. a) Positive correlation displays dynamic change of state transitions. Proportion of k_{max}-core voxel IC-composition on dynamic study is not reflected on static study, which is indicated by the stacked bar plot in the left lower hand. b) Negative correlation shows relatively smooth progression with pulses without significant state transitions. Proportion of k_{max}-core voxel IC-composition on dynamic study is reflected on static study, which is indicated by the stacked bar plot in the left lower hand.

Comparison of static and dynamic hierarchical structures

Hierarchical structure derived from static and dynamic studies were compared to determine the characteristics of dynamic study. As seen in the categorization of patterns of k_{max}-core voxels-IC composition, the compositions were similar in the static and dynamic studies in negative correlation. k_{max}-core voxels-IC composition in dynamic study revealed dynamic change over time, but when assessed in the overall entire time bin, the composition was similar as static study. Thus, composition and its ratio of k_{max}-core voxels-IC on static study were reflected on dynamic study (Fig. 4B). This enables predicting overall k_{max}-core voxels-IC composition in dynamic study from the static study and predicting the composition of k_{max}-core voxels in static study from dynamic study, vice versa.

However, this pattern was not evidently observed in the positive correlation, and the proportion of k_{max}-core voxels-IC composition was variable between dynamic and static study (Fig. 4A). Animated stacked histogram of k_{max}-core voxels-IC composition revealed dynamic and diverse change of its composition over time, and the composition of static study was not able to capture its dynamic change. Therefore, predicting the dynamic hierarchical structure was not possible from static hierarchical structure in positive correlation.

Visual assessment of coreness k value map

Coreness k values of voxels representing the position of each voxel in the hierarchical structure from dynamic and static studies were rendered over

transaxial image of brain T1 MRI to visualize the distribution of coreness *k* value more intuitively, expressing more details, such as right or left sidedness of the coreness *k* value which was not well described on flag plot or stacked histogram. The color bar scale was set as 95% of individual k_{max}-core. 36 transaxial images of coreness *k* value overlayed on brain T1 MRI were merged to evaluate the distribution of coreness *k* value at a glance (Fig. 5, Movie. S4). Dynamic coreness *k* values from both positive and negative correlations were summed in the same individual to assess the whole functional intervoxel connectivity in both positive and negative-influence networks. As seen on the previous plots, dynamic change in distribution of coreness *k* value was observed over time, which was not fully reflected on static coreness *k* map. Distribution and its change differed among individuals.

It is evident that static coreness *k* value cannot reflect the dynamic coreness *k* value that appear at certain time bin, but dynamic coreness *k* value from the entire time bins (116 or 93) were summed to investigate the relationship with the static coreness *k* value. Coreness *k* value map of summed dynamic study was compared with static study visually and revealed that the distribution of coreness *k* values were similar on both studies (Fig. 5).

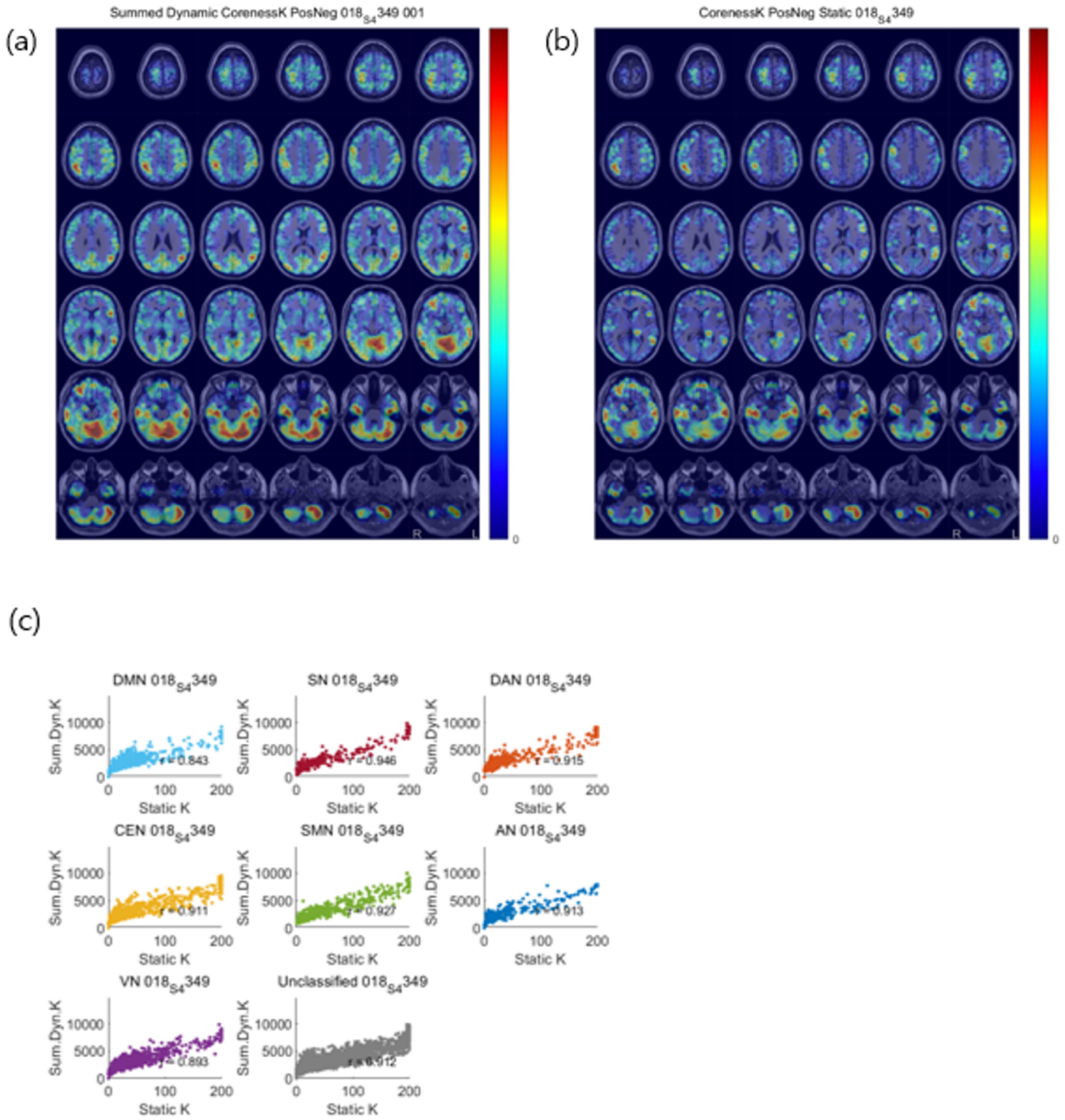

Fig 5. Visual and quantitative assessment of summed dynamic coreness *k* map and static coreness *k* map in aged HC subject (F/71.5). Dynamic (a) and static (b) coreness *k* map display similar distribution of coreness *k* values and the high correlation between two studies are confirmed by the correlation plot.

Figure 6. Visual and quantitative assessment of summed dynamic coreness *k* map and static coreness *k* map in positive and negative correlations. Overall similarities are observed between two maps in positive (a) and negative (b) correlations, confirmed by positive correlation in all IC-maps. Intensity of the summed dynamic coreness *k* map is higher than static coreness *k* map, especially in negative correlation and this finding is confirmed with steeper slope on correlation plot.

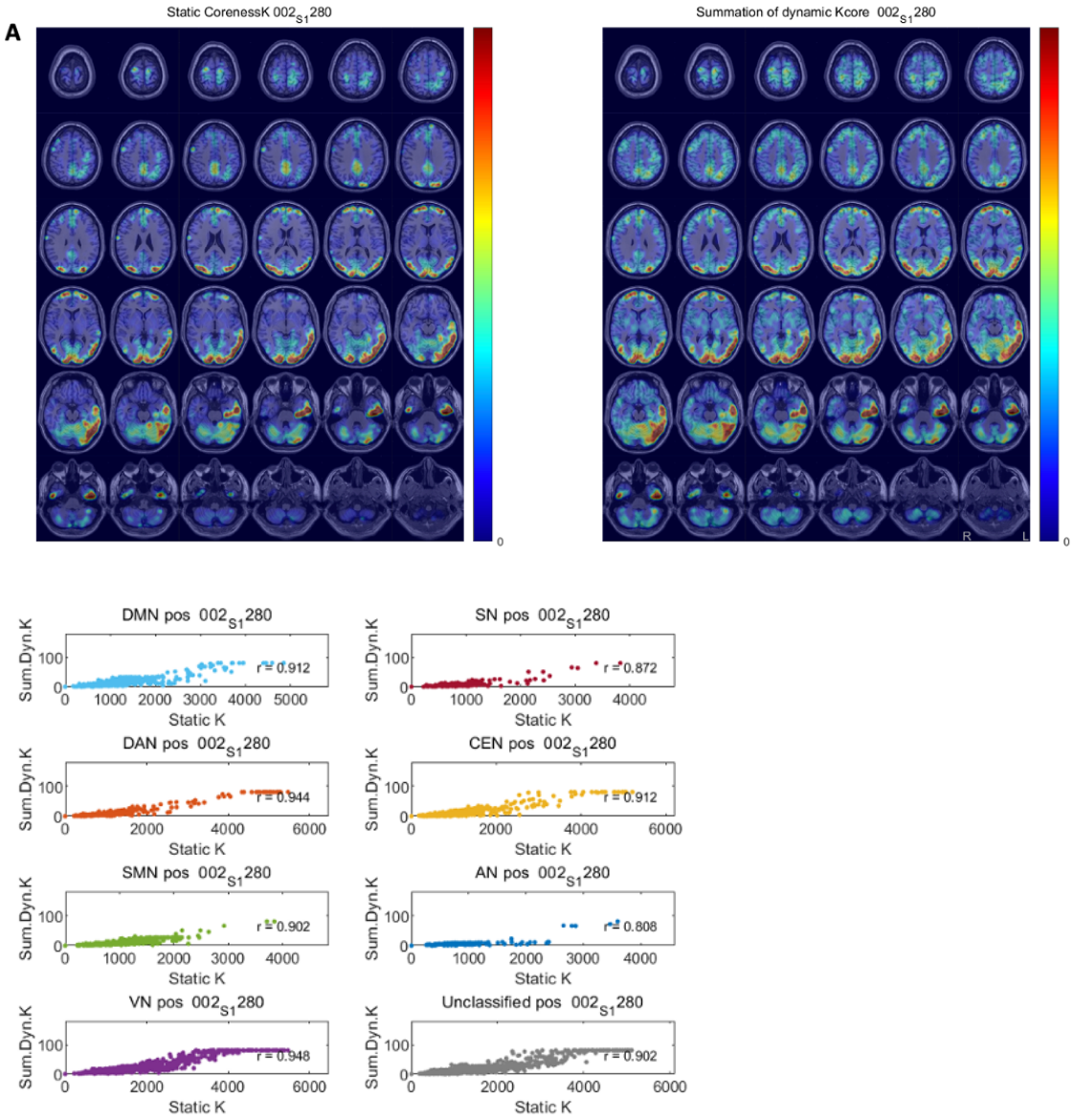

B

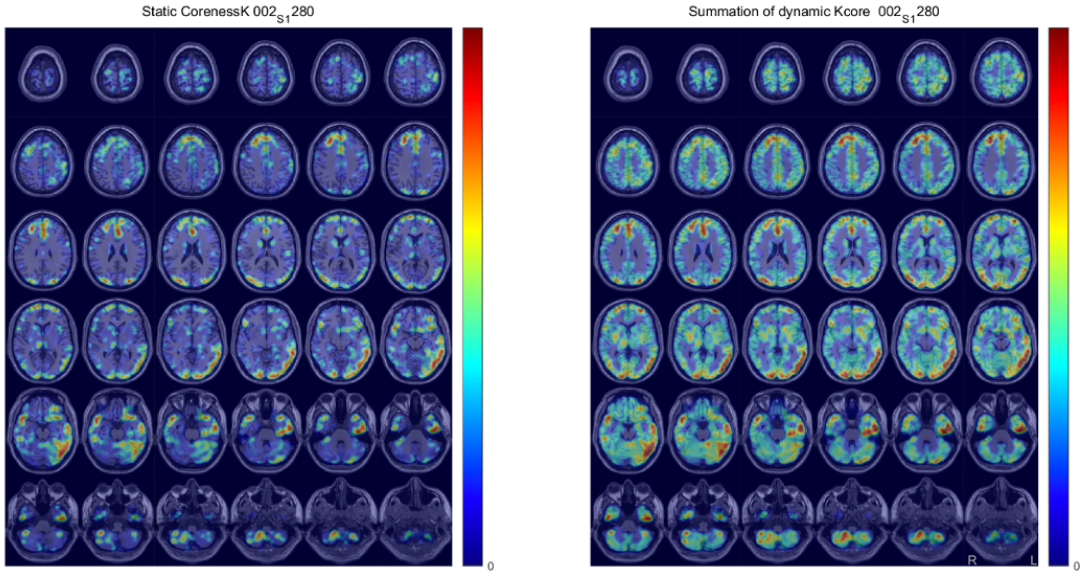

Negative Correlation

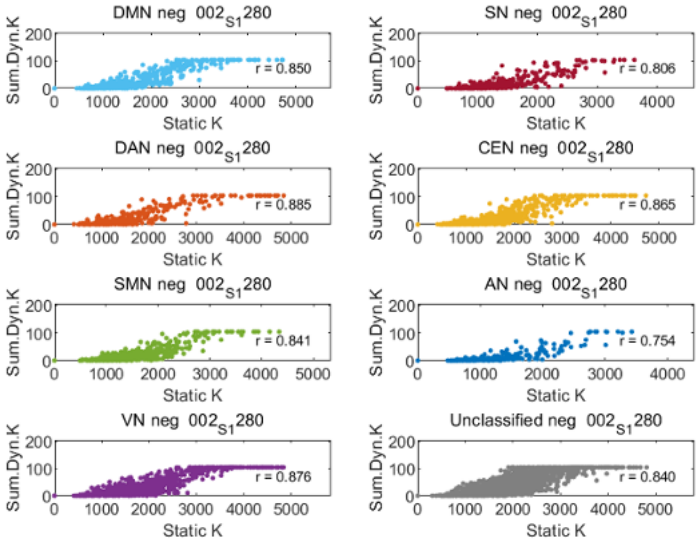

Minor difference did exist in the intensity of coreness *k* value in specific brain regions, but the overall distribution of coreness *k* values were similar. So, the dynamic coreness *k* values may differ along the time but when summed altogether, it is similar as the static coreness *k* value which is derived from the entire time bin.

To confirm the visual similarity objectively, quantitative assessment was performed between the summed dynamic and static coreness *k* values in the designated IC-maps. As the visual assessment, correlation plots between summed dynamic and static coreness *k* values displayed high positive correlation. Even in the classified IC-based analysis, these values were positively correlated in all regions (Fig. 5C). Thus, sum of dynamic coreness *k* value from entire time bins can be considered to reflect the static coreness *k* value.

In addition, in the visual analysis, the overall intensity of coreness *k* value map seemed to be higher on the summed dynamic coreness *k* map than static coreness *k* map, especially in negative correlation. Correlation plot validated the visual finding by displaying steeper slope on the correlation plot (Fig. 6) in negative correlations compared to the positive correlations.

Comparison of dynamic coreness k map in positive and negative correlations

Dynamic coreness *k* value map was rendered in positive and negative correlation in the same individual, to compare the distribution of coreness *k* values in both

correlations (Movie. S5), which displayed different flow pattern of dynamic hierarchical structure on animated flag plot and stacked histogram. On dynamic coreness k map, change of distribution of coreness k values on brain were both diverse in positive and negative correlations with different patterns from each other. While the dynamic change of k_{max}-core voxels-IC composition revealed state transitions or smooth progressions in the flow pattern, distinguishing positive and negative correlations, dynamic coreness k map exhibited temporal change of distribution of coreness k values without displaying significant similarity or difference in both correlations. This implies that intervoxel correlation in positive and negative influence is dynamic over time in the brain, and its dynamic change is diverse without exhibiting characteristic pattern in both correlations.

Comparison of dynamic coreness k map in young and aged groups

Although there was inter-individual variability in the distribution of coreness k values, a specific pattern was noticed to characterize the young and aged groups, which was not evidently observed on previous plots of k_{max}-core voxels-IC compositions. In yHC group, overall change of distribution was symmetric and the transition of coreness k values showed diffuse symmetric, synchronized movement. However, despite the same normal cognition, aHC showed rather asymmetric distribution of coreness k value in the brain (Fig 7, Movie. S6). This pattern was recognizable both on static and dynamic studies,

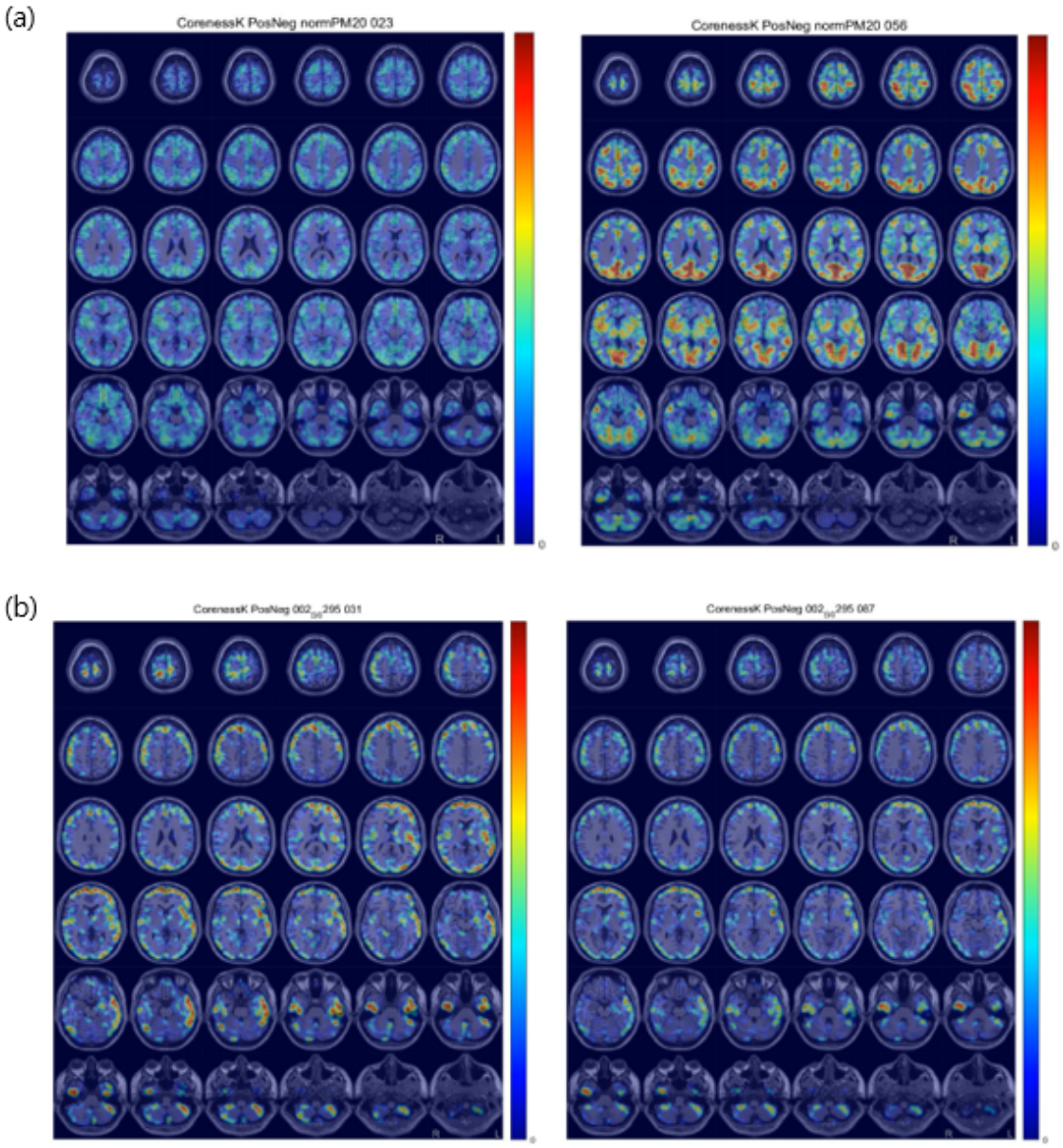

Figure 7. Coreness *k* value maps of summed dynamic positive-negative correlations in young and aged HC subjects: yHC (M/25) (a), aHC (M/90) (b) (a) Diffuse symmetric, synchronized distribution of dynamic coreness *k* values is observed in the young healthy control subject. (b) Relatively uneven, asymmetric distribution of dynamic coreness *k* values is noted in the old healthy control subject.

and in positive and negative correlations. It is implied that aging process led to altered distribution and transition of coreness k values. Tendency of asymmetric, unsynchronized distribution seemed to be prominent as the aging progressed.

Quantitative assessment with asymmetry index

Asymmetric distribution of coreness k values detected on coreness k map was evaluated with asymmetry index for quantitative and objective assessment. Brain regions were divided into left and right, anatomically with 11 brain regions of interest (ROI: hemisphere, prefrontal cortex, somatomotor cortex, parietal, temporal, cingulate, insula, limbic, basal ganglia thalamus, visual, cerebellum) or functionally with 7 IC maps (DMN, SN, DAN, CEN, SMN, AN, VN), and the asymmetry indexes (AI) were calculated in these regions. Box plots were generated to visualize the difference of asymmetry index among groups.

Asymmetry index from static studies were evaluated between young and aged healthy control groups, and the absolute value of asymmetry index tended to increase as the subject's age increased. Among 11 brain ROIs, ROIs such as cingulate, insula, limbic, visual regions showed statistically significant difference (Table 3, Fig. 8A, 8B).

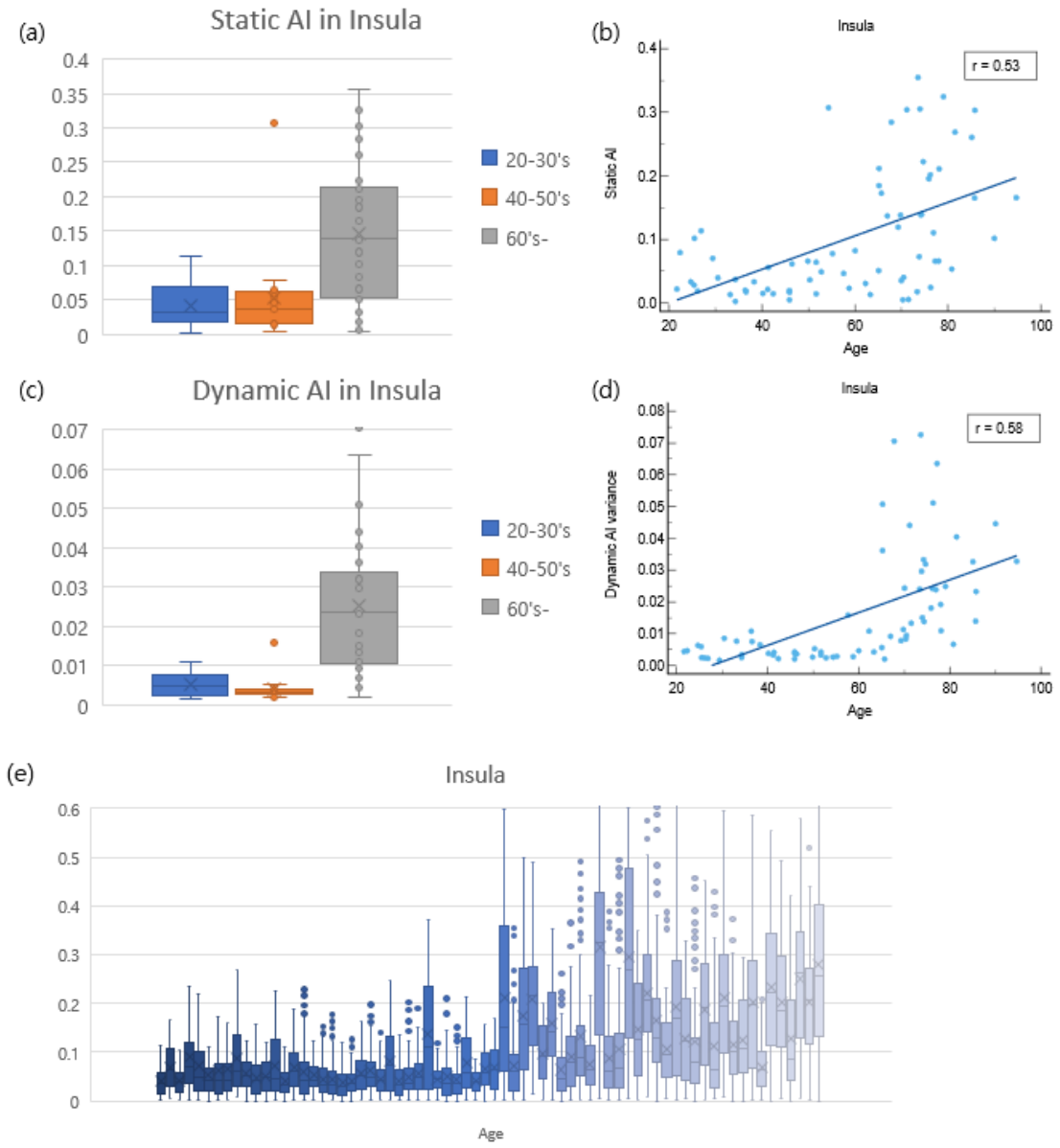

Figure 8. Asymmetry index in insula on static and dynamic studies. (a) Static asymmetry index of aged HC over 60 years old show greater range of asymmetry index than young HC. (b) Static AI is increased as the age increased. (c) Variance of dynamic asymmetry index is greatest in the aged HC over 60 years old. (d) Dynamic AI variance is positively correlated with age, increasing significantly over age 60. (e) As the age is increased, variance of dynamic asymmetry index also increased.

Table 3. Comparison of static AI in ROI according to age.

ROI	20-30's (n=15)	40-50's (n=17)	60's(n=38)	P value
Hemisphere	0.015 ± 0.011	0.020 ± 0.022	0.0245 ± 0.018	0.113
PFC	0.030 ± 0.022	0.028 ± 0.030	0.045 ± 0.041	0.243
SMC	0.025 ± 0.021	0.039 ± 0.026	0.053 ± 0.045	0.069
Parietal	0.040 ± 0.029	0.035 ± 0.030	0.067 ± 0.069	0.349
Temporal	0.022 ± 0.019	0.031 ± 0.023	0.043 ± 0.038	0.070
Cingulate	0.061 ± 0.033	0.089 ± 0.037	0.010 ± 0.047	0.021*
Insula	0.042 ± 0.033	0.053 ± 0.069	0.147 ± 0.103	<0.001*
Limbic	0.033 ± 0.033	0.026 ± 0.021	0.076 ± 0.070	0.002*
BG Thalamus	0.024 ± 0.013	0.023 ± 0.020	0.084 ± 0.079	<0.001*
Visual	0.019 ± 0.015	0.020 ± 0.022	0.069 ± 0.052	<0.001*
Cerebellum	0.041 ± 0.026	0.037 ± 0.024	0.061 ± 0.048	0.274

* P value less than 0.05 is considered statistically significant

Table 4. Comparison of variance of dynamic AI in ROI according to age

ROI	20-30's (n=15)	40-50's (n=17)	60's (n=38)	P value
Hemisphere	0.0001 ± 0.0004	0.0003 ± 0.0004	0.0008 ± 0.0005	<0.001*
PFC	0.002 ± 0.001	0.001 ± 0.001	0.003 ± 0.002	<0.001*
SMC	0.002 ± 0.001	0.002 ± 0.001	0.005 ± 0.003	<0.001*
Parietal	0.002 ± 0.0001	0.002 ± 0.001	0.006 ± 0.005	<0.001*
Temporal	0.002 ± 0.001	0.002 ± 0.002	0.006 ± 0.003	<0.001*
Cingulate	0.002 ± 0.002	0.001 ± 0.001	0.006 ± 0.005	<0.001*
Insula	0.005 ± 0.003	0.004 ± 0.003	0.025 ± 0.019	<0.001*
Limbic	0.003 ± 0.002	0.003 ± 0.002	0.014 ± 0.012	<0.001*
BG Thalamus	0.002 ± 0.001	0.002 ± 0.001	0.010 ± 0.007	<0.001*
Visual	0.002 ± 0.002	0.001 ± 0.001	0.006 ± 0.006	<0.001*
Cerebellum	0.003 ± 0.002	0.001 ± 0.001	0.006 ± 0.004	<0.001*

* P value less than 0.05 is considered statistically significant

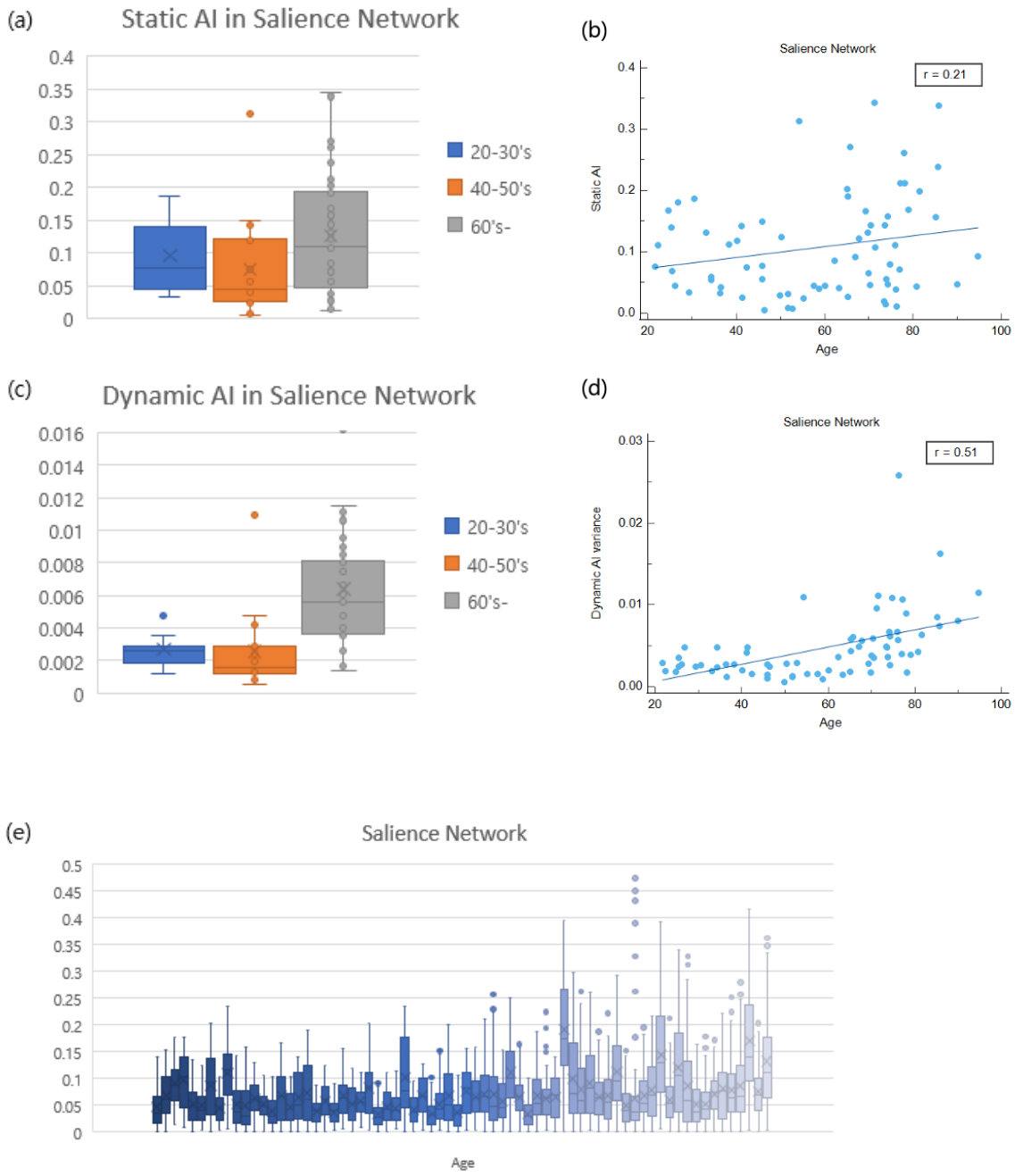

Figure 9. Asymmetry index in SN on static and dynamic studies. (a) Static asymmetry index of aged HC over 60 years old show greater range of asymmetry index than young HC. (b) Static AI is increased as the age increased. (c) Variance of dynamic asymmetry index is greatest in the aged HC over 60 years old. (d) Dynamic AI variance is positively correlated with age, particularly increasing over age 60. (e) As the age is increased, variance of dynamic asymmetry index also increased.

When the asymmetry index was assessed in 7 IC maps, similar result was observed. Between young and aged healthy control groups, several IC regions such as SN, SMN, AN, VN showed statistically significant difference (Table S1, Fig. 9A).

Asymmetry index from dynamic study displayed prominent difference between young and aged healthy control groups, as well. Regions identified with statistical significance on static asymmetry index were investigated with more caution in dynamic asymmetry index. As the age increased in the normal cognitive group, change of asymmetry index in a subject also increased in the same regions as the static study. To express the dynamic change of asymmetry index, variance of asymmetry index over time in each subject was generated. Variance revealed similar pattern as the static asymmetry index, variance increased as the age increased. Significant difference was observed in the ROIs of yHC group compared to aHC group (Table 4, Fig. 8B).

In comparison with static asymmetry index, variance of dynamic asymmetry index displayed the difference between groups more clearly. While static asymmetry index of ROIs and IC maps revealed statistical significance in some regions, variance of dynamic asymmetry index displayed evident difference in all regions of ROI and IC maps, except CEN, between young and aged healthy control groups (Table S2, Fig. 9B).

Correlation of age and coreness k values

Coreness k values derived from static and dynamic studies were evaluated and the voxel-wise correlation between coreness k values and age was assessed. Static and dynamic coreness k values were classified into 7 IC regions. Correlation between age and coreness k values in each IC regions was assessed. Coreness k values from age 20 to 60 remained in plateau, but at the age of 60, coreness k values from both static and dynamic studies tended to drop dramatically in all IC regions (Fig. 10). Regression analysis was performed in the whole group between age and coreness k value and revealed high negative correlation in all IC regions with r value of 0.6.

Coreness k values in gender and aging

It has been noted in previous studies that gender may affect brain connectivity and aging (54, 55, 56, 57, 58, 59), so the k_{max}-core voxels and coreness k values were also compared between male and female. Despite some previous studies suggesting difference in genders, no significant difference was detected in the hierarchical core voxels of both k_{max}-core voxels and coreness k values. There was no significant difference in the pattern or composition of k_{max}-core voxels and quantity or asymmetry index of coreness k values (Fig. 11).

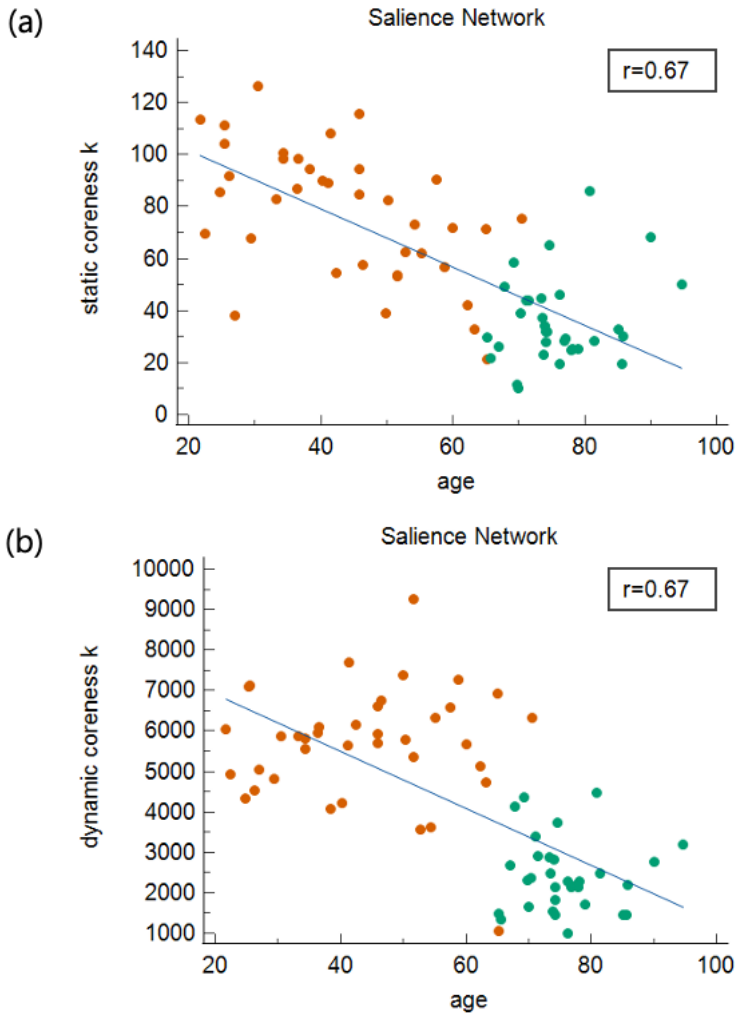

Figure 10. Correlation of age and IC-based coreness *k* values in salience network.

Orange dots represent SNU data and green dots represent ADNI data. Decrease of static (a) and dynamic (b) coreness *k* values over age is displayed on scatter plots.

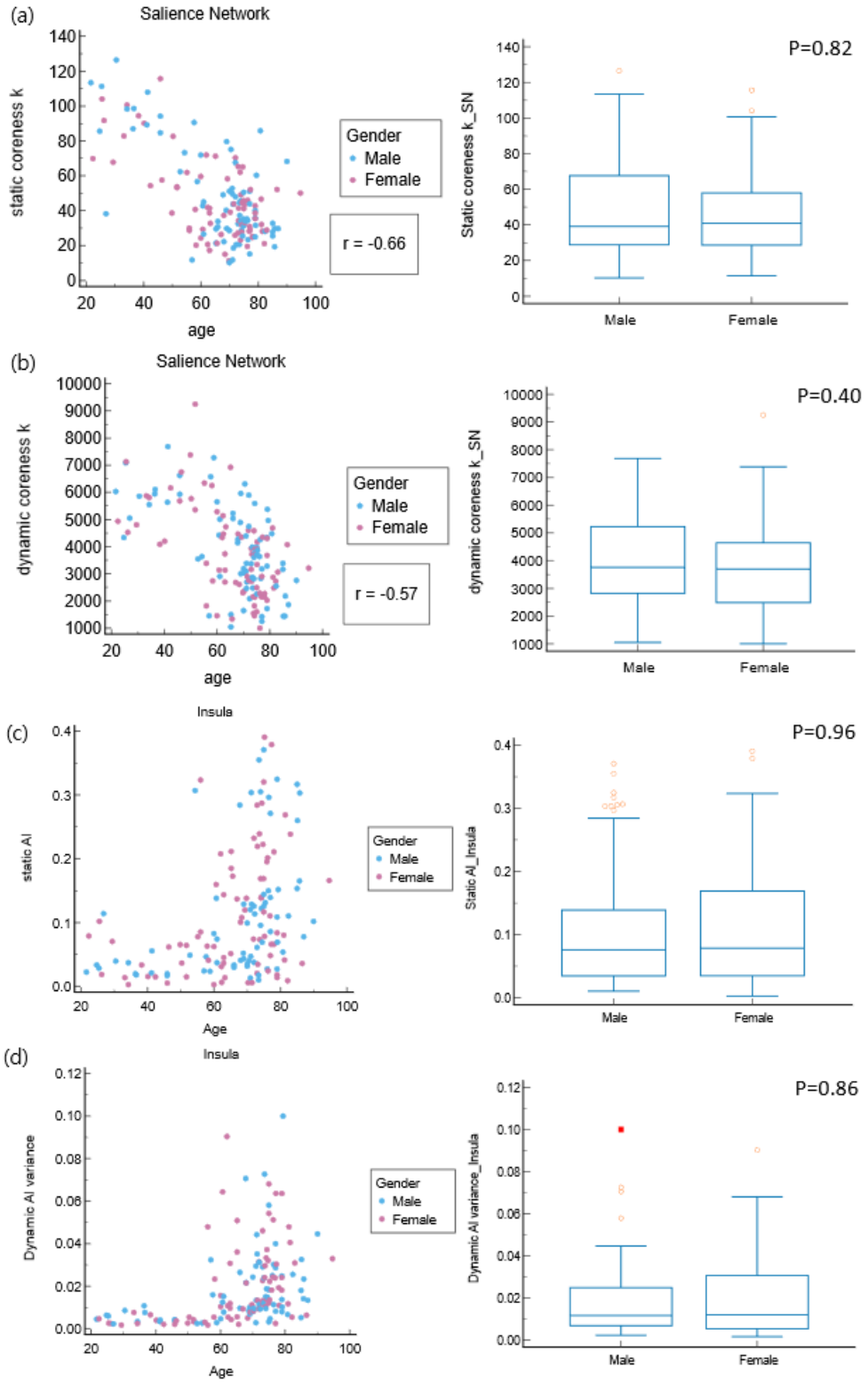

Figure 11. Correlation of age and gender in SN and insula. No significant difference is noted between male and female in static (a) and dynamic (b) coreness *k* values. Asymetry index in insula was also similar in static (c) and dynamic (d) studies.

Validation of coreness k values in young group

Results have suggested that coreness *k* values differ according to age, with high coreness *k* values and low asymmetry index in young age but one flaw in this study is that these data are retrieved from different database. Since ADNI data is comprised of aged population with or without cognitive impairment, relatively young population have not been included in the study database.

So data of young normal cognitive population from Human Connectome Project (HCP, https://www.humanconnectome.org/) was additionally processed as supplement independent set to validate the results in young healthy control group. 30 normal healthy contols with average age of 29.1 (23.5 to 38) without any significant history of psychiatric disorder, neurological or cardiovascular disease were included. rsfMRI data were preprocessed in the similar manner as the SNU and ADNI data, using smoothing with 6mm full-width at half maximum of Gaussian kernel, bandpass filtering (0.01 Hz – 0.1 Hz). Temporal filtering with 0.01 to 0.1 Hz and downsampling were applied, and total 5,937 voxels were included for analysis with 6 x 6 x 6 mm^3.

HCP data revealed similar results as SNU data. There was inter-individual variability in the IC-composition of k_{max}-core voxels but symmetric distribution of coreness *k* map with low asymmetry index was observed and coreness *k* values in static and dynamic studies showed high value compared to aged population as well (Fig. 12). Thus, it can be concluded that young normal population exhibit

similar functional connectivity and that aging deteriorates asymmetry and decrease in connectivity.

DISCUSSION

k-core percolation analysis in the dynamic study of rsfMRI successfully revealed dynamic hierarchical structure of functional intervoxel connectivity on voxel-level, displaying dynamic change in the composition of coreness *k* values of voxels and identifying voxels with uppermost hierarchy at certain time points, which may represent the most influential voxel at one's brain function at the moment (30, 31). Dynamic and static functional connectivity revealed by *k*-core percolation analysis were compared and disclosed that the static study cannot fully reflect the dynamic nature of the brain function, thus implying that it is more reasonable to study the brain function in dynamic basis rather than static basis.

For dynamic analysis of functional intervoxel connectivity, sliding window methods have been used in the previous studies with various protocols. Spatial units ranged from voxels (1 mm^3) to voxels-of-interest (VOIs; hundreds or more of voxels). In HMM analysis, these voxels were aggregated to make states and a few to dozen state units were used for interpretation, which was consisted of thousands or more voxels (8,9). In CAP analysis, which is a seeds-based analysis, the seeds were also made of thousands of voxels (13-15). These methods aggregated voxels to analyze, assuming that the VOIs are spatially homogeneous. This is considered limitation of these methods, since VOIs are heterogeneous.

In this study, *k*-core percolation method was used, which is a method using the voxel as the input to overcome this weakness. Voxel itself was put into analysis pipe, and these voxels were not aggregated in the process. About 20 million

neurons are estimated to exist as excitatory or inhibitory neurons in 6x6x6 mm^3 of brain cortex (27), which is the voxel size used in this analysis. Thus, voxel itself still can be heterogeneous. To overcome the heterogeneity of the voxel, sufficient observations is needed to decrease intervoxel variations. In this study, 1-minute was chosen as the time unit in the sliding window method, and 2-seconds shift in ADNI and SNU data generated 116 time-bins or 93 time-bins, respectively. 1-minute time bin assumes that the neuronal interaction within this voxel is stationary. Small time shifts, in this case, 1 step, partially overlaps two successive windows to observe time-varying change. It was to resolve the problem of possible heterogeneity within the voxel by increasing the number of observations. This strategy of defining voxels and time-bins of 1 minute as inputs revealed the dynamic change of compositions of IC-based k_{max}-core voxels and the distribution of coreness k value over time. Generated figures and animations enabled visual and quantitative assessment of dynamic hierarchical structures of functional intervoxel connectivity, facilitating understanding of an individual's brain function, particularly in the aging process.

Recent investigation in single cell transcriptomics combined neuronal cell clusters to classify these cluster into hierarchical groups of 32 neuronal types. In this hierarchical structure, excitatory and inhibitory neurons form diverse types of clusters, and many clusters overlapped each other (60). 20 million neurons per voxel units were analyzed to reveal the hierarchical structures of positive and negative correlations, which are assumed to represent the excitatory and inhibitory networks (61). In this study, excitatory network was assessed as positive correlation by generating connectivity matrix of each window to conduct

k-core percolation, with thresholds meeting scale-freeness. Inhibitory network was assessed with using the absolute values derived from negative correlation, which went through thresholding with scale-freeness and *k*-core percolation, as well. Coreness *k* values from negative correlation were visualized and compared in the same way as the positive correlation analysis. Dynamic coreness *k* values from positive and negative correlations were summed to integrate the excitatory and inhibitory networks in the assessment of dynamic functional connectivity (61).

Dynamic study is clearly different from the static study and the static study cannot fully reflect the time-varying characteristics observed in the dynamic study. By the various plots generated in this study, it is clear that hierarchical structure of voxels changes dynamically along time. Nevertheless, when these time-varying changes of dynamic coreness *k* values from the entire time bins were summed altogether, it was similar with static coreness *k* values.

To confirm the visual similarities between the summed dynamic and static coreness *k* value maps, correlation plot in two studies was carried out (Fig. 5). Correlation plot revealed positive correlation in all regions of IC maps, confirming the similarities between summed dynamic and static coreness *k* value distributions. Therefore, it can be implied that even though dynamic coreness *k* value at certain time bin may be diverse and unique, when these values are added altogether, summed dynamic coreness *k* value is eventually the same as the static coreness *k* value measured from the entire time bin, and that static coreness *k* values connote the information from dynamic coreness *k* values.

Dynamic hierarchical structure of coreness k values in positive and negative correlations exhibited different flow pattern along the time, portraying different dynamic functional state. More diverse change of IC-based voxel compositions was noted in the positive correlation. Abrupt state transition was commonly observed (83%) and more diverse types of IC-based voxel composition were present. These abrupt state transitions are assumed to represent the dynamic spikes of excitatory signals in an individual. Change of IC-based voxel composition over time was too diverse on dynamic study that composition of static study failed to reflect the composition of dynamic study in positive correlation.

In contrast, flow pattern in negative correlation was somewhat monotonous from positive correlation. In general, abrupt change of state was less observed, mostly displaying smooth progression (87%) in distributed pattern (79%), with persisting certain combination of states throughout some time or entire time bins. In addition, UNC-based voxels tended to exist in considerable portion throughout the whole phase in negative correlation. From the monotonous progress over time, inhibitory signals can be assumed to be present in more stable state than excitatory signals without significant change of IC-based voxels over time. Due to its stable pattern, IC-based voxel composition of dynamic study was reflected on static study. Hence, prediction of composition on dynamic study from static study was possible.

Although, dominant composition of dynamic study is reflected on the static study in negative correlation with monotonous progress, there is limitation in assessing

dynamic study from static study. Coreness k value from static study is derived from the whole acquired time, while dynamic coreness k values are derived from certain 1-min time bins in the whole acquired time. A composition at certain time bin may have been similar with static study composition, but in another time, composition can be totally different. Examples are well presented in the positive correlations. Thus, static study cannot fully reflect the diversity of dynamic study and playing limited role in interpreting the time-varying change of brain function, so assessing dynamic studies is essential to investigate the brain function of an individual.

Visualization of coreness k value map over brain MRI was more effective in investigating the distribution of coreness k value on the brain, both in dynamic and static studies. While right or left sidedness of coreness k value was not expressed on flag plots or stacked histogram, coreness k value map visualized the distribution of these values with directionality, revealing certain features in the distribution of coreness k values.

To evaluate the feasibility of k-core percolation method in clinical fields, analysis was applied to assess the change of hierarchical structures of core voxels in the aging process of normal cognition population. While no distinctive characteristics were discovered on dynamic hierarchical structure plotted on animated flag plots or stacked histograms, dynamic coreness k value map revealed certain pattern that may aid in distinguishing young individual from aged individual and possibly providing further insight in the hierarchical structure change in aging process. Temporal change of distribution of coreness k value on coreness k map was

synchronized with symmetric distribution in the yHC group. However, aHC group displayed the dissociative flow change with asymmetric distribution, which may indicate aging may be the factors affecting functional intervoxel connectivity. The finding was consistent in positive, negative correlations and in both correlations combined.

Static coreness *k* value map also displayed similar pattern as dynamic coreness *k* value map. yHC group showed diffuse symmetric distribution of coreness *k* values and aHC group tended to show asymmetric distribution. Asymmetry or dissociative-ness was less prominent in static coreness *k* map than the dynamic coreness *k* map in aHC group, but it was enough to easily identify that the distribution is clearly different from the yHC group.

To assess the visual asymmetry of distribution detected on coreness *k* map more objectively, asymmetry index was applied to quantitatively assess the asymmetric distribution of coreness k values. Brain regions were divided into left and right to assess the asymmetry index in the regions classified anatomically (ROI) and functionally (IC). Asymmetry index was calculated by $|(left-right)/(left+right)*0.5|$.

Static asymmetry index identified several regions with statistically significant asymmetry. The identified brain regions in ROI and IC were similar, such as insula and SN, somatomotor cortex and SMN, visual cortex and VN. These regions were considered as independent set in analyzing the dynamic asymmetry index. Besides identifying regions affected by asymmetry, static asymmetry index

distinguished yHC from aHC group, which was consistent with finding on coreness k map, with significantly lower asymmetry index in yHC group.

Based on the findings from static asymmetry index, asymmetry index was assessed in the dynamic studies. To assess the change of asymmetry index over time, variance of dynamic asymmetry index was calculated to evaluate the dispersed asymmetry index over time in a subject. More dispersed values meant more fluctuating asymmetry indexes over time. When the change of asymmetry index over time in a subject was arranged in the order of age, the tendency of increasing extent of dispersed asymmetry index in a subject was noted as the age increased. This finding was confirmed by assessing variance in the young and aged HC groups statistically. While static asymmetry index was significantly different in some regions, variance of dynamic asymmetry index was significantly different in all regions except CEN.

Previous studies have indicated asymmetry in functional connectivity in aging or cognitive impairment as part of aging process in the brain (47, 49, 50, 62, 63, 64, 65, 66, 67). The results are not consistent, but it seems that asymmetry does play a role in aging. As some part of brain network's function decline, other part may be activated for compensation (49, 50), or functional connectivity can be decreased in the regions known to be vulnerable to structural atrophy occurring in the aging process (39, 66). Various regions or networks in the brain were affected by asymmetry, such as DMN, DAN, SN, insula (66, 67, 68). In this study, asymmetry was significantly correlated with aging in the similar regions or networks identified in previous studies.

Decreased connectivity in the aging process has been investigated in various studies (38, 40, 42, 59, 66, 68, 69, 70). Generally, it is considered that overall connectivity is decreased in the elderly but connectivity in some regions may be increased by the compensation process. Previous studies have assessed brain connectivity as ROI-based approach, calculating connectivity with one-dimensional edge in the ROI. In this study, brain connectivity has been assessed in voxel-level using degree-based nodes, so voxel with higher value of k meant higher connectivity within nodes. Thus, decreasing connectivity in aging has been confirmed by decrease in coreness k values in 7 IC regions. Both in static and dynamic studies, the coreness k values tended to maintain or mildly decrease until the age of 60, when the coreness k values dropped. This implies that brain connectivity maintains its integrity in the adulthood but tends to lose it when the individual enters the seniorhood.

Despite these findings, there are some limitations in this study. First, despite the efforts to reduce the heterogeneity of the analytic unit by using the voxel as the unit, voxel itself consists of millions of neurons, which connotes heterogeneity. In this study, the number of observations was increased to decrease the heterogeneity of the voxels, but further action may be needed to reduce heterogeneity to increase the overall integrity of the k-core percolation method. Second, the thresholds set to fit the scale-freeness was applied in each group with fixed value. Applying the adequate threshold for each individual may be more appropriate to generate the optimal binary adjacency matrices. Lastly, although there were efforts to quantitate the visual findings, more methods to assess the

findings objectively should be developed for further clinical application, such as in interpreting the change of K_{max}-core voxels on flag plots or stacked histograms.

CONCLUSION

This study disclosed the integrity of the k-percolation method in the assessment of dynamic hierarchical structure on voxel-level from rsfMRI and its utility in investigating aging process more intuitively. Dynamic hierarchical structure was effectively visualized on various plots. Comparing with static functional connectivity confirmed that it is more appropriate to investigate dynamic functional connectivity for better understanding an individual's brain function due to its dynamic nature. Also, this method displayed possibility of clinical application in detecting abnormalities of dynamic functional connectivity in the brain on individual basis.

REFERENCES

1. Smitha KA, Akhil Raja K, Arun KM, Rajesh PG, Thomas B, Kapilamoorthy TR, et al. Resting state fMRI: A review on methods in resting state connectivity analysis and resting state networks. Neuroradiol J. 2017;30(4):305-17.

2. Liégeois R, Li J, Kong R, Orban C, Van De Ville D, Ge T, et al. Resting brain dynamics at different timescales capture distinct aspects of human behavior. Nat Commun. 2019;10(1):2317.

3. Allen EA, Damaraju E, Plis SM, Erhardt EB, Eichele T, Calhoun VD. Tracking whole-brain connectivity dynamics in the resting state. Cereb Cortex. 2014;24(3):663-76.

4. Chang C, Glover GH. Time-frequency dynamics of resting-state brain connectivity measured with fMRI. Neuroimage. 2010;50(1):81-98.

5. Handwerker DA, Roopchansingh V, Gonzalez-Castillo J, Bandettini PA. Periodic changes in fMRI connectivity. Neuroimage. 2012;63(3):1712-9.

6. Hutchison RM, Womelsdorf T, Allen EA, Bandettini PA, Calhoun VD, Corbetta M, et al. Dynamic functional connectivity: promise, issues, and interpretations. Neuroimage. 2013;80:360-78.

7. Jones DT, Vemuri P, Murphy MC, Gunter JL, Senjem ML, Machulda MM, et al. Non-stationarity in the "resting brain's" modular architecture. PLoS One. 2012;7(6):e39731.

8. Kiviniemi V, Vire T, Remes J, Elseoud AA, Starck T, Tervonen O, et al. A sliding time-window ICA reveals spatial variability of the default mode network in time. Brain Connect. 2011;1(4):339-47.

9. O'Neill GC, Tewarie P, Vidaurre D, Liuzzi L, Woolrich MW, Brookes MJ. Dynamics of large-scale electrophysiological networks: A technical review. Neuroimage. 2018;180(Pt B):559-76.

10. Menon SS, Krishnamurthy K. A Comparison of Static and Dynamic Functional Connectivities for Identifying Subjects and Biological Sex Using Intrinsic Individual Brain Connectivity. Sci Rep. 2019;9(1):5729.

11. Calhoun VD, Miller R, Pearlson G, Adalı T. The chronnectome: time-varying connectivity networks as the next frontier in fMRI data discovery. Neuron. 2014;84(2):262-74.

12. Chen JE, Rubinov M, Chang C. Methods and Considerations for Dynamic Analysis of Functional MR Imaging Data. Neuroimaging Clin N Am. 2017;27(4):547-60.

13. Jie B, Liu M, Shen D. Integration of temporal and spatial properties of dynamic connectivity networks for automatic diagnosis of brain disease. Med Image Anal. 2018;47:81-94.

14. Deco G, Vidaurre D, Kringelbach ML. Revisiting the global workspace orchestrating the hierarchical organization of the human brain. Nat Hum Behav. 2021;5(4):497-511.

15. Vidaurre D. A new model for simultaneous dimensionality reduction and time-varying functional connectivity estimation. PLoS Comput Biol. 2021;17(4):e1008580.

16. Vidaurre D, Abeysuriya R, Becker R, Quinn AJ, Alfaro-Almagro F, Smith SM, et al. Discovering dynamic brain networks from big data in rest and task. Neuroimage. 2018;180(Pt B):646-56.

17. Vidaurre D, Llera A, Smith SM, Woolrich MW. Behavioural relevance of spontaneous, transient brain network interactions in fMRI. Neuroimage. 2021;229:117713.

18. Vidaurre D, Smith SM, Woolrich MW. Brain network dynamics are hierarchically organized in time. Proc Natl Acad Sci U S A. 2017;114(48):12827-32.

19. Liu X, Chang C, Duyn JH. Decomposition of spontaneous brain activity into distinct fMRI co-activation patterns. Front Syst Neurosci. 2013;7:101.

20. Liu X, Zhang N, Chang C, Duyn JH. Co-activation patterns in resting-state fMRI signals. Neuroimage. 2018;180(Pt B):485-94.

21. Tagliazucchi E, von Wegner F, Morzelewski A, Brodbeck V, Laufs H. Dynamic BOLD functional connectivity in humans and its electrophysiological correlates. Front Hum Neurosci. 2012;6:339.

22. Vitiello G. The use of many-body physics and thermodynamics to describe the dynamics of rhythmic generators in sensory cortices engaged in memory and learning. Curr Opin Neurobiol. 2015;31:7-12.

23. Cavanna F, Vilas MG, Palmucci M, Tagliazucchi E. Dynamic functional connectivity and brain metastability during altered states of consciousness. Neuroimage. 2018;180(Pt B):383-95.

24. Roberts JA, Gollo LL, Abeysuriya RG, Roberts G, Mitchell PB, Woolrich MW, et al. Metastable brain waves. Nat Commun. 2019;10(1):1056.

25. Tognoli E, Kelso JA. The metastable brain. Neuron. 2014;81(1):35-48.

26. Torres JJ, Marro J. Brain Performance versus Phase Transitions. Sci Rep. 2015;5:12216.

27. Keller D, Erö C, Markram H. Cell Densities in the Mouse Brain: A Systematic Review. Front Neuroanat. 2018;12:83.

28. Pervaiz U, Vidaurre D, Gohil C, Smith SM, Woolrich MW. Multi-dynamic modelling reveals strongly time-varying resting fMRI correlations. Med Image Anal. 2022;77:102366.

29. Zhang X, Maltbie EA, Keilholz SD. Spatiotemporal trajectories in resting-state FMRI revealed by convolutional variational autoencoder. Neuroimage. 2021;244:118588.

30. Whi W, Huh Y, Ha S, Lee H, Kang H, Lee DS. Characteristic functional cores revealed by hyperbolic disc embedding and k-core percolation on resting-state fMRI. Sci Rep. 2022;12(1):4887.

31. Huh Y, Kang YK, Whi W, Lee H, Kang H, Lee DS. Time-varying hierarchical core voxels disclosed by k-core percolation on dynamic inter-voxel connectivity resting-state fMRI. biorxiv: CSH; 2022.

32. Martínez-Murcia FJ, Górriz JM, Ramírez J, Puntonet CG, Illán IA, Initiative AsDN. Functional activity maps based on significance measures and Independent Component Analysis. Comput Methods Programs Biomed. 2013;111(1):255-68.

33. Young PNE, Estarellas M, Coomans E, Srikrishna M, Beaumont H, Maass A, et al. Imaging biomarkers in neurodegeneration: current and future practices. Alzheimers Res Ther. 2020;12(1):49.

34. Arbizu J, Festari C, Altomare D, Walker Z, Bouwman F, Rivolta J, et al. Clinical utility of FDG-PET for the clinical diagnosis in MCI. Eur J Nucl Med Mol Imaging. 2018;45(9):1497-508.

35. Pievani M, Filippini N, van den Heuvel MP, Cappa SF, Frisoni GB. Brain connectivity in neurodegenerative diseases--from phenotype to proteinopathy. Nat Rev Neurol. 2014;10(11):620-33.

36. Hohenfeld C, Werner CJ, Reetz K. Resting-state connectivity in neurodegenerative disorders: Is there potential for an imaging biomarker? Neuroimage Clin. 2018;18:849-70.

37. Filippi M, Basaia S, Canu E, Imperiale F, Meani A, Caso F, et al. Brain network connectivity differs in early-onset neurodegenerative dementia. Neurology. 2017;89(17):1764-72.

38. Varangis E, Habeck CG, Razlighi QR, Stern Y. The Effect of Aging on Resting State Connectivity of Predefined Networks in the Brain. Front Aging Neurosci. 2019;11:234.

39. Liu X, Chen X, Zheng W, Xia M, Han Y, Song H, et al. Altered Functional Connectivity of Insular Subregions in Alzheimer's Disease. Front Aging Neurosci. 2018;10:107.

40. Brewster BM, Pasqualini MS, Martin LE. Functional Brain Connectivity and Inhibitory Control in Older Adults: A Preliminary Study. Front Aging Neurosci. 2022;14:763494.

41. Prvulovic D, Bokde AL, Faltraco F, Hampel H. Functional magnetic resonance imaging as a dynamic candidate biomarker for Alzheimer's disease. Prog Neurobiol. 2011;95(4):557-69.

42. Tomasi D, Volkow N. Aging and functional brain networks. Molecular Psychiatry; 2012. p. 549–58.

43. Greicius MD, Srivastava G, Reiss AL, Menon V. Default-mode network activity distinguishes Alzheimer's disease from healthy aging: evidence from functional MRI. Proc Natl Acad Sci U S A. 2004;101(13):4637-42.

44. Bai F, Zhang Z, Yu H, Shi Y, Yuan Y, Zhu W, et al. Default-mode network activity distinguishes amnestic type mild cognitive impairment from healthy aging: a combined structural and resting-state functional MRI study. Neurosci Lett. 2008;438(1):111-5.

45. Agosta F, Pievani M, Geroldi C, Copetti M, Frisoni GB, Filippi M. Resting state fMRI in Alzheimer's disease: beyond the default mode network. Neurobiol Aging. 2012;33(8):1564-78.

46. Koch W, Teipel S, Mueller S, Benninghoff J, Wagner M, Bokde AL, et al. Diagnostic power of default mode network resting state fMRI in the detection of Alzheimer's disease. Neurobiol Aging. 2012;33(3):466-78.

47. Sun Y, Li J, Suckling J, Feng L. Asymmetry of Hemispheric Network Topology Reveals Dissociable Processes between Functional and Structural Brain Connectome in Community-Living Elders. Front Aging Neurosci. 2017;9:361.

48. Levman J, Fang Z, Zumwalt K, Cogger L, Vasung L, MacDonald P, et al. Asymmetric Insular Connectomics Revealed by Diffusion Magnetic Resonance Imaging Analysis of Healthy Brain Development. Brain Connect. 2019;9(1):2-12.

49. Hill C, Van Gemmert AWA, Fang Q, Hou L, Wang J, Pan Z. Asymmetry in the aging brain: A narrative review of cortical activation patterns and implications for motor function. Laterality. 2020;25(4):413-29.

50. Li Z, Moore AB, Tyner C, Hu X. Asymmetric connectivity reduction and its relationship to "HAROLD" in aging brain. Brain Res. 2009;1295:149-58.

51. Glasser MF, Sotiropoulos SN, Wilson JA, Coalson TS, Fischl B, Andersson JL, et al. The minimal preprocessing pipelines for the Human Connectome Project. Neuroimage. 2013;80:105-24.

52. Whi W, Ha S, Kang H, Lee DS. Hyperbolic disc embedding of functional human brain connectomes using resting-state fMRI. Network Neuroscience: The MIT Press; 2022. p. 745 - 64.

53. Azimi-Tafreshi N, Gómez-Gardeñes J, Dorogovtsev SN. k-core percolation on multiplex networks. Phys Rev E Stat Nonlin Soft Matter Phys. 2014;90(3):032816.

54. Gong G, Rosa-Neto P, Carbonell F, Chen ZJ, He Y, Evans AC. Age- and gender-related differences in the cortical anatomical network. J Neurosci. 2009;29(50):15684-93.

55. Sie JH, Chen YH, Shiau YH, Chu WC. Gender- and Age-Specific Differences in Resting-State Functional Connectivity of the Central Autonomic Network in Adulthood. Front Hum Neurosci. 2019;13:369.

56. Nephew BC, Febo M, Cali R, Workman KP, Payne L, Moore CM, et al. Robustness of sex-differences in functional connectivity over time in middle-aged marmosets. Sci Rep. 2020;10(1):16647.

57. Lopez-Larson MP, Anderson JS, Ferguson MA, Yurgelun-Todd D. Local brain connectivity and associations with gender and age. Dev Cogn Neurosci. 2011;1(2):187-97.

58. Zhang C, Dougherty CC, Baum SA, White T, Michael AM. Functional connectivity predicts gender: Evidence for gender differences in resting brain connectivity. Hum Brain Mapp. 2018;39(4):1765-76.

59. Malpetti M, Ballarini T, Presotto L, Garibotto V, Tettamanti M, Perani D, et al. Gender differences in healthy aging and Alzheimer's Dementia: A. Hum Brain Mapp. 2017;38(8):4212-27.

60. Hodge RD, Bakken TE, Miller JA, Smith KA, Barkan ER, Graybuck LT, et al. Conserved cell types with divergent features in human versus mouse cortex. Nature. 2019;573(7772):61-8.

61. Moon HS, Jiang H, Vo TT, Jung WB, Vazquez AL, Kim SG. Contribution of Excitatory and Inhibitory Neuronal Activity to BOLD fMRI. Cereb Cortex. 2021;31(9):4053-67.

62. Wu X, Wu Y, Geng Z, Zhou S, Wei L, Ji GJ, et al. Asymmetric Differences in the Gray Matter Volume and Functional Connections of the Amygdala Are Associated With Clinical Manifestations of Alzheimer's Disease. Front Neurosci. 2020;14:602.

63. Stark SM, Frithsen A, Stark CEL. Age-related alterations in functional connectivity along the longitudinal axis of the hippocampus and its subfields. Hippocampus. 2021;31(1):11-27.

64. Roe JM, Vidal-Piñeiro D, Sørensen Ø, Brandmaier AM, Düzel S, Gonzalez HA, et al. Asymmetric thinning of the cerebral cortex across the adult lifespan is accelerated in Alzheimer's disease. Nat Commun. 2021;12(1):721.

65. Liang L, Yuan Y, Wei Y, Yu B, Mai W, Duan G, et al. Recurrent and concurrent patterns of regional BOLD dynamics and functional connectivity dynamics in cognitive decline. Alzheimers Res Ther. 2021;13(1):28.

66. Daianu M, Jahanshad N, Nir TM, Toga AW, Jack CR, Weiner MW, et al. Breakdown of brain connectivity between normal aging and Alzheimer's disease: a structural k-core network analysis. Brain Connect. 2013;3(4):407-22.

67. Yang C, Zhong S, Zhou X, Wei L, Wang L, Nie S. The Abnormality of Topological Asymmetry between Hemispheric Brain White Matter Networks in Alzheimer's Disease and Mild Cognitive Impairment. Front Aging Neurosci. 2017;9:261.

68. Cansino S. Brain connectivity changes associated with episodic recollection decline in aging: A review of fMRI studies. Front Aging Neurosci. 2022;14:1012870.

69. Schulz M, Mayer C, Schlemm E, Frey BM, Malherbe C, Petersen M, et al. Association of Age and Structural Brain Changes With Functional Connectivity and Executive Function in a Middle-Aged to Older Population-Based Cohort. Front Aging Neurosci. 2022;14:782738.

70. Farras-Permanyer L, Mancho-Fora N, Montalà-Flaquer M, Bartrés-Faz D, Vaqué-Alcázar L, Peró-Cebollero M, et al. Age-related changes in resting-state functional connectivity in older adults. Neural Regen Res. 2019;14(9):1544-55.

Figure S1. Selected 7 independent components in group ICA (31).

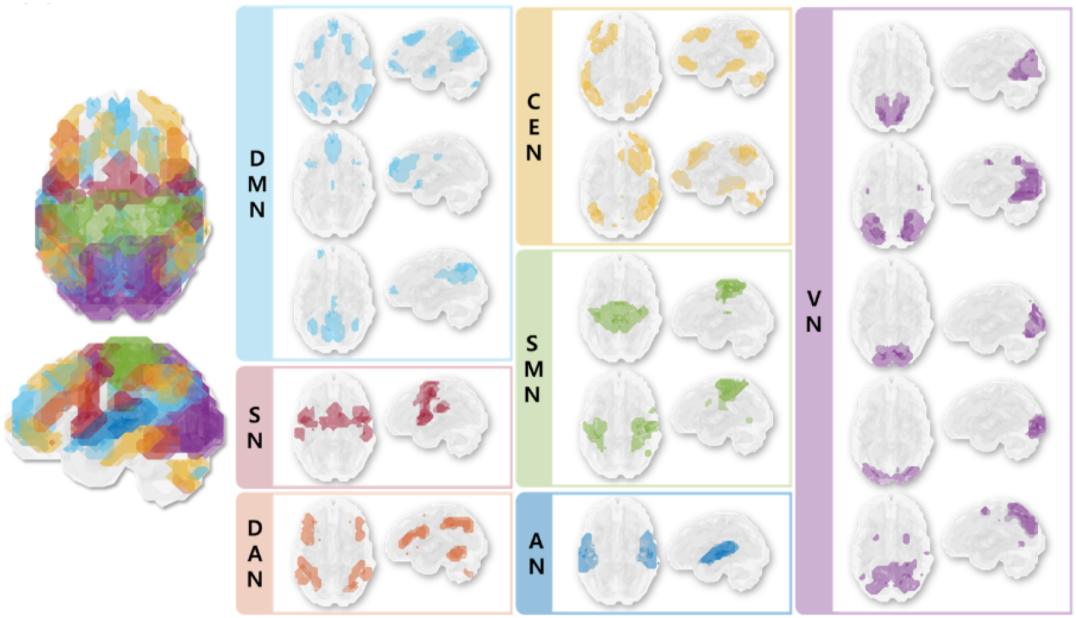

Figure S2. Flow patterns of positive and negative correlations in static and dynamic study in young HC group

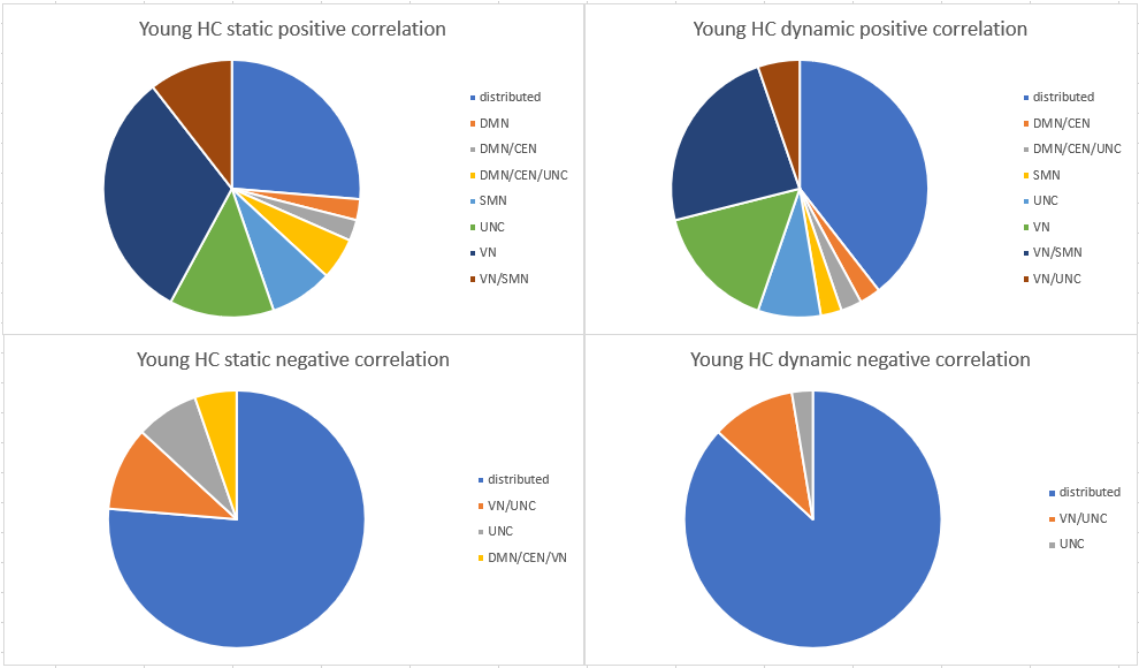

Figure S3. Validation of young normal data with HCP data. HCP data expressed as orange dots, SNU and ADNI data expressed as blue dots. Young individuals from HCP and SNU data show similar distribution of static (a) and dynamic (b) coreness *k* values and static (c) and dynamic (d) asymmetry indexes. Demographics of HCP data shown on table (e)

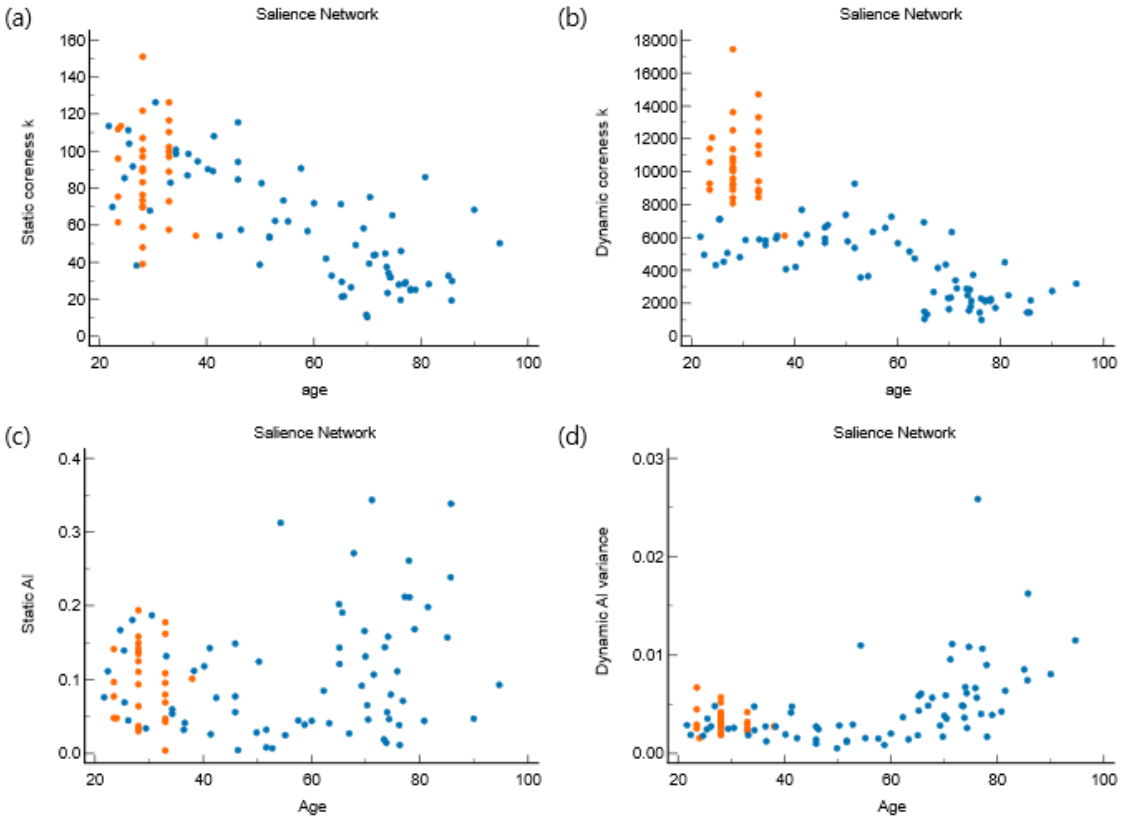

(e)

	HCP
Number	30
Age	29.1 ± 3.6 (23.5 - 38)
Sex (M:F)	16:14
MMSE	28.80 ± 1.17

Table S1. Comparison of static asymmetry index in IC according to age

IC	20-30's (n=15)	40-50's (n=17)	Aged normal (n=38)	P value
DMN	0.114 ± 0.050	0.115 ± 0.059	0.137 ± 0.07437	0.349
SN	0.096 ± 0.055	0.075 ± 0.078	0.126 ± 0.089	0.039*
DAN	0.326 ± 0.085	0.322 ± 0.093	0.295 ± 0.167	0.491
CEN	0.219 ± 0.085	0.191 ± 0.072	0.174 ± 0.090	0.245
SMN	0.075 ± 0.059	0.083 ± 0.079	0.131 ± 0.111	0.144
AN	0.072 ± 0.060	0.085 ± 0.081	0.136 ± 0.108	0.087
VN	0.055 ± 0.034	0.048 ± 0.049	0.134 ± 0.106	0.087

* P value less than 0.05 is considered statistically significant

Table S2. Comparison of variance of dynamic asymmetry index in IC according to age

IC	20-30's (n=15)	40-50's (n=17)	Aged normal (n=38)	P value
DMN	0.002 ± 0.001	0.002 ± 0.001	0.003 ± 0.002	<0.001*
SN	0.003 ± 0.001	0.003 ± 0.002	0.006 ± 0.005	<0.001*
DAN	0.002 ± 0.001	0.003 ± 0.004	0.007 ± 0.005	<0.001*
CEN	0.003 ± 0.001	0.002 ± 0.002	0.003 ± 0.002	0.072
SMN	0.002 ± 0.003	0.002 ± 0.001	0.006 ± 0.003	<0.001*
AN	0.003 ± 0.002	0.004 ± 0.006	0.010 ± 0.007	<0.001*
VN	0.002 ± 0.001	0.001 ± 0.001	0.004 ± 0.004	<0.001*

* P value less than 0.05 is considered statistically significant

Movie S1. Dynamic hierarchical structure plotted on various plots in young HC subject. (a) Dynamic change of IC-compositions of k_{max}-core voxels in positive correlation is visualized on animated brain-rendered image, stacked histogram. Animated brain-rendered image displays k_{max}-core voxels in designated IC-colors, roughly showing the distribution over the brain. (b) Time-varying change of k_{max}-core voxels IC-compositions on stacked histogram are visualized simulataneously on animated flag plots and barplots. In this case of positive correlation, various state transitions and pulses are observed along the time.

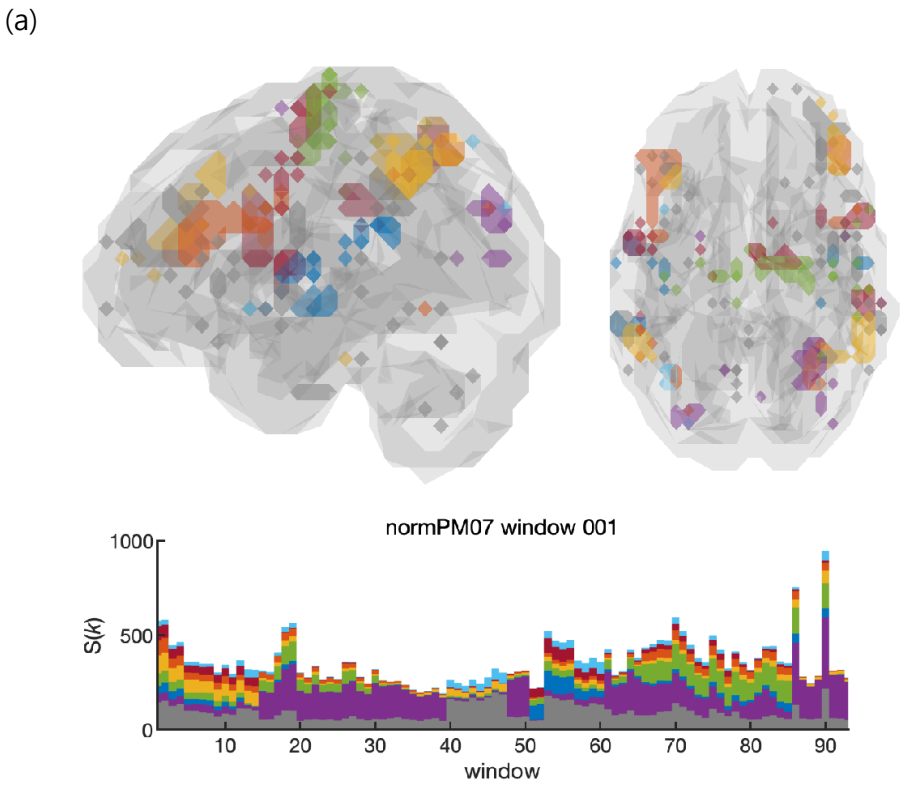

(b)

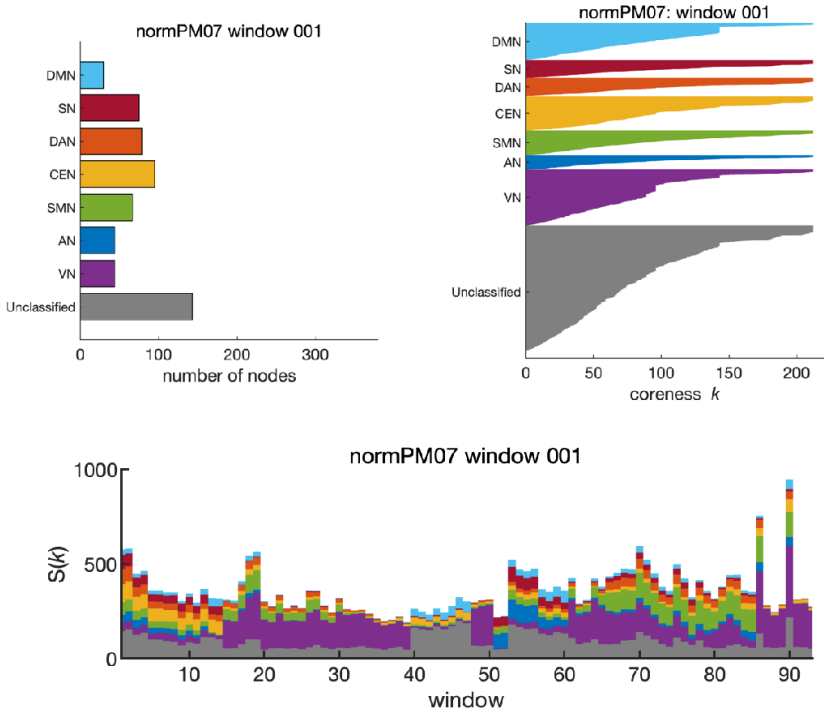
normPM07 window 001
DMN
SN
DAN
CEN
SMN
AN
VN
Unclassified
0
100
200
300
number of nodes
normPM07: window 001
DMN
SN
DAN
CEN
SMN
AN
VN
Unclassified
0
50
100
150
200
coreness k
normPM07 window 001
1000
500
0
S(k)
10
20
30
40
50
60
70
80
90
window

Movie S2. Static k_{max}-core voxels and dynamic k_{max}-core voxels and coreness k values in positive correlation. (a) Dynamic change of state, state transitions, pulses are well visualized in positive correlation of aged HC subject. (b) Dynamic change of IC-composition of k_{max}-core voxels is not reflected on the stacked bar plot of static k_{max}-core voxels.

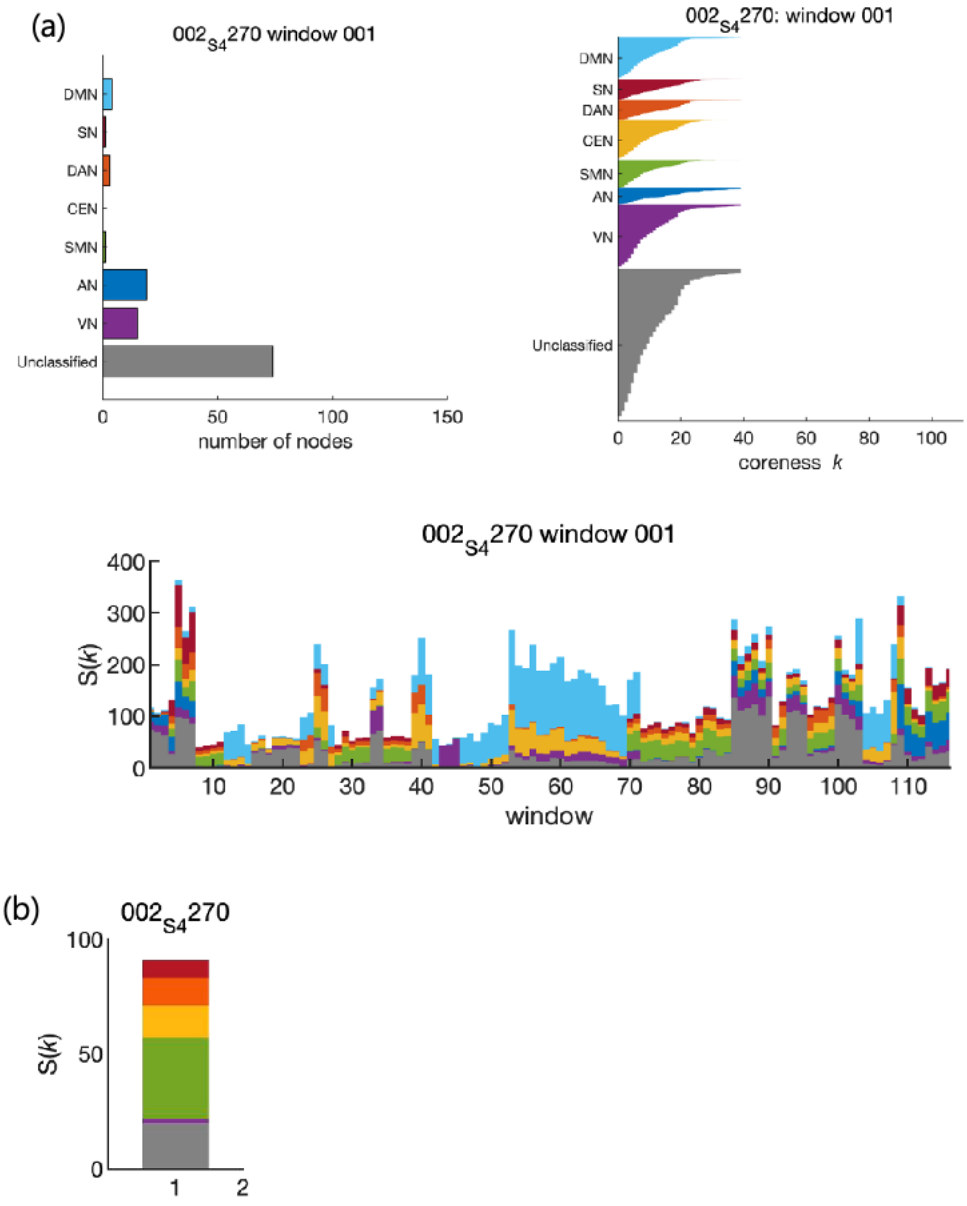

Movie S3. Static k_{max}-core voxels and dynamic k_{max}-core voxels and coreness k values in negative correlation. (a) Smooth progression with distributed pattern is well visualized in negative correlation of aged HC subject. (b) IC-composition of k_{max}-core voxels in dynamic change is well reflected on the stacked bar plot of static k_{max}-core voxels.

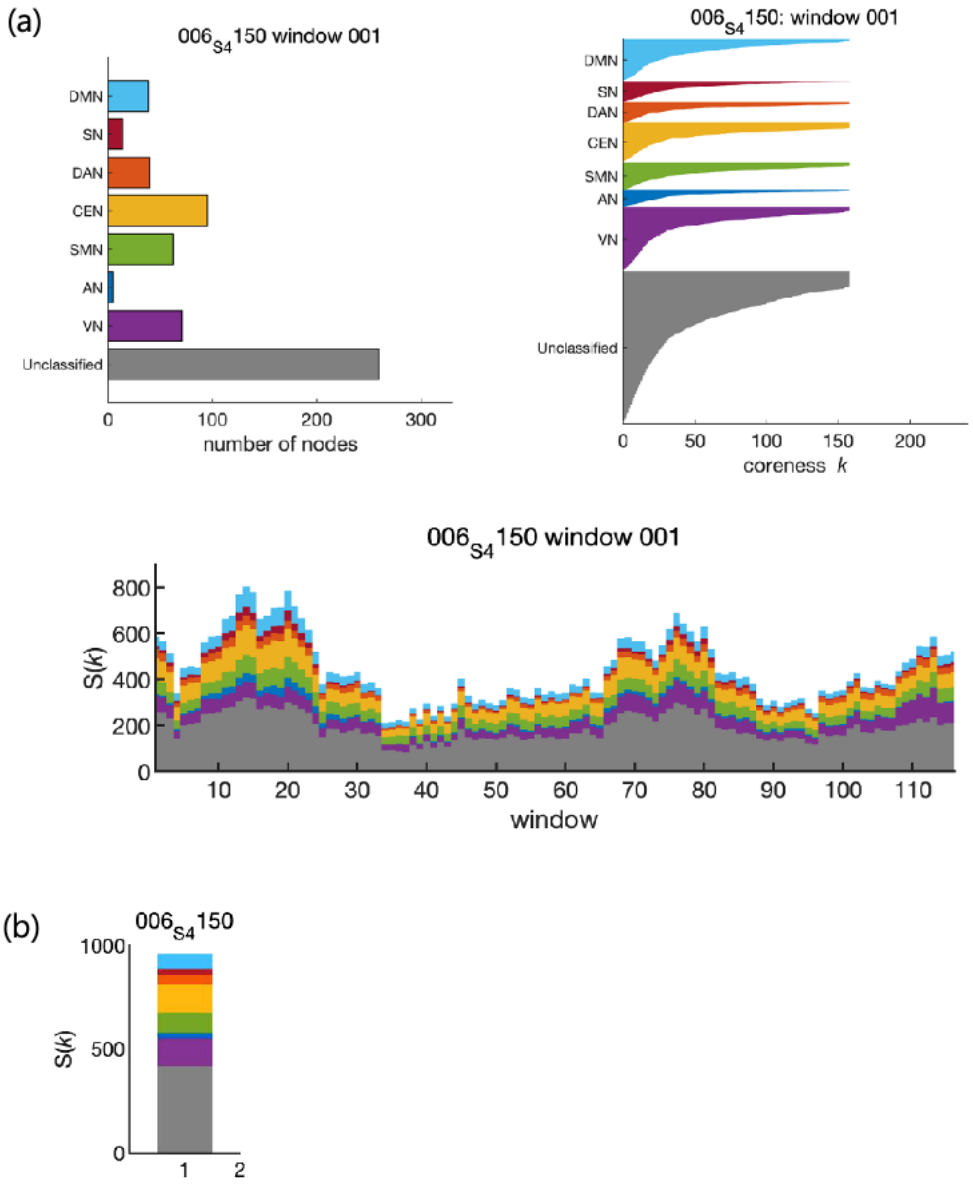

Movie S4. Coreness *k* value maps in dynamic (a), static (b) studies of summed positive and negative correlations in aged HC subject (F/71.5). Distribution of dynamic coreness *k* value varies along time.

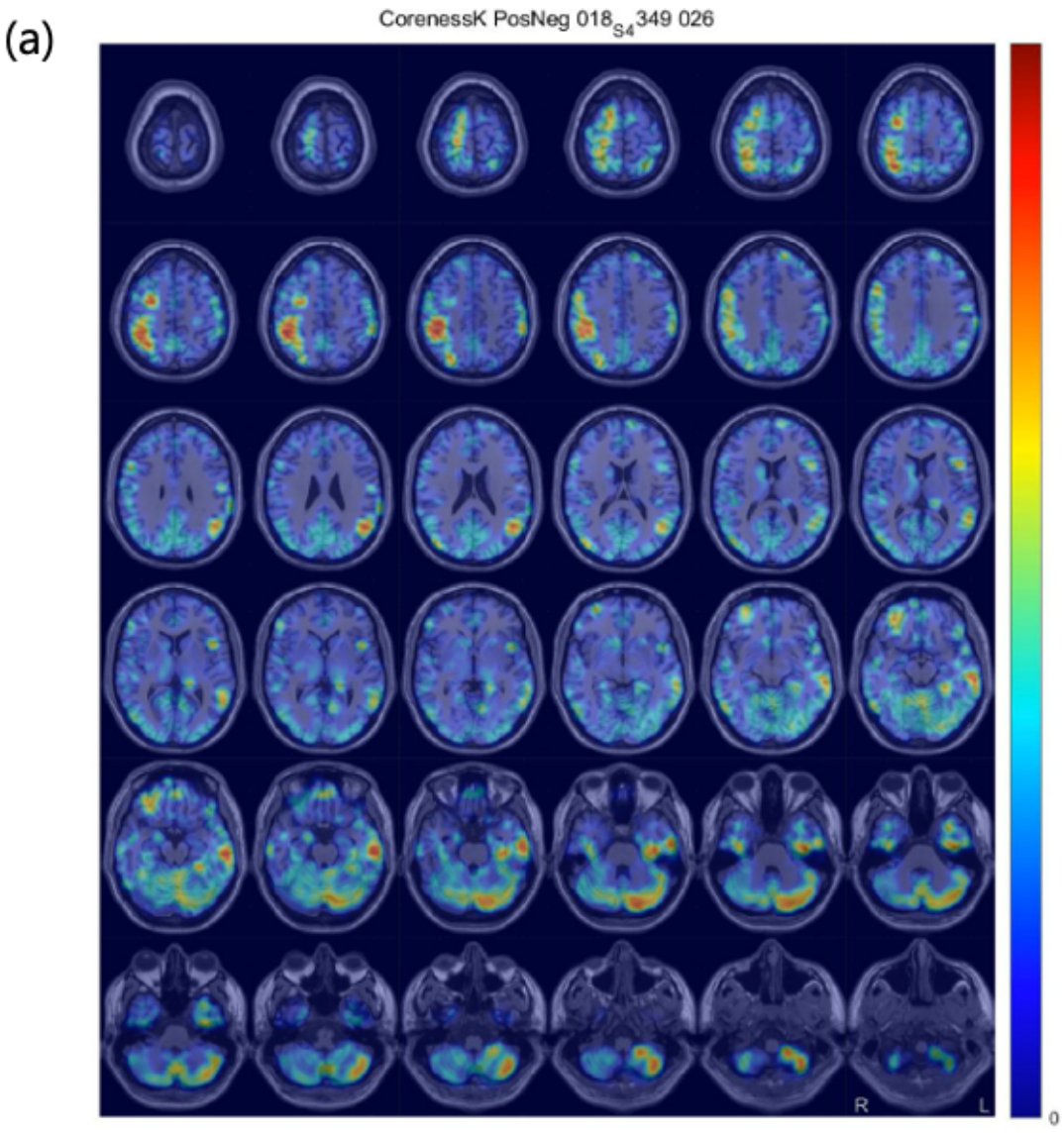

(b)

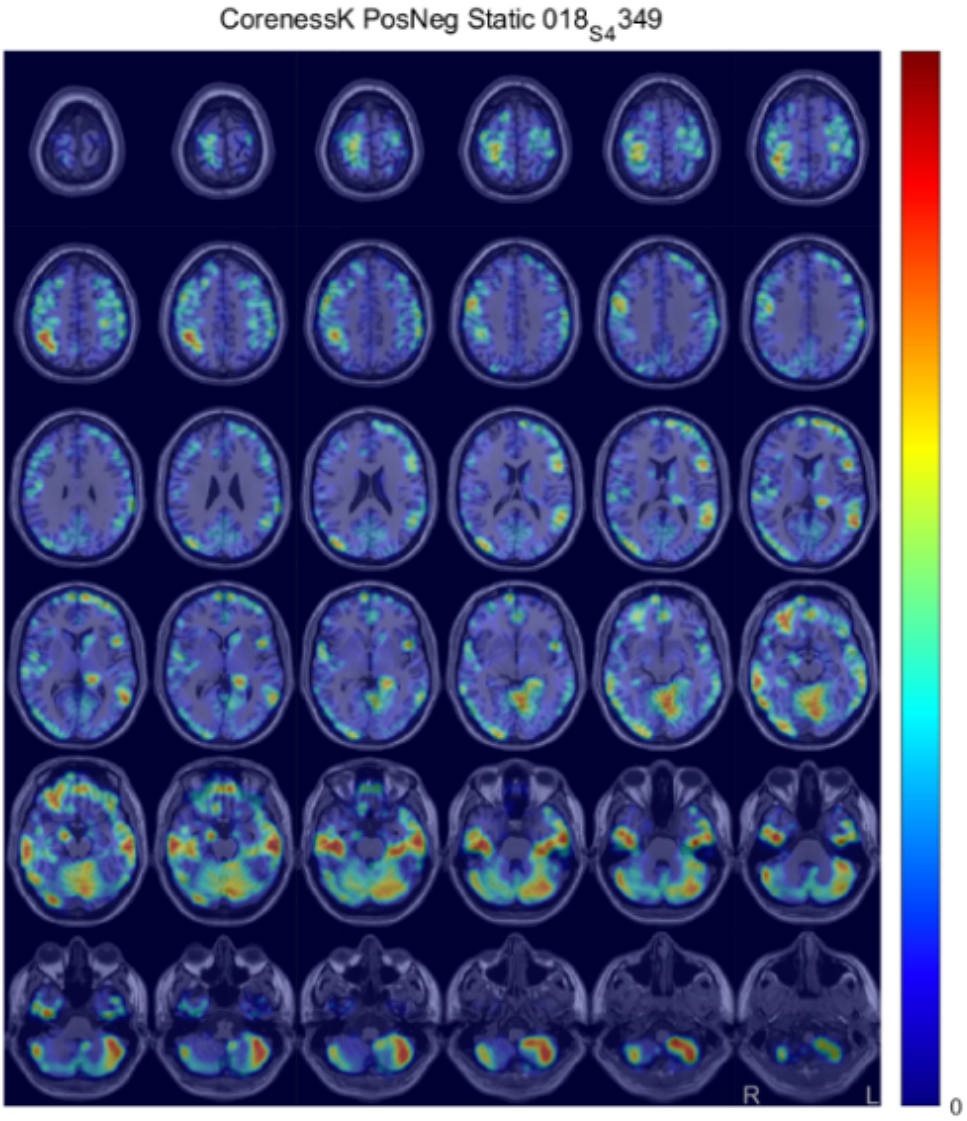

Movie S5. Dynamic coreness *k* value maps in positive (a) and negative (b) correlations in aged HC subject (F/77.2). Similar but different pattern of distribution of dynamic coreness *k* values is observed in positive and negative correlation in an aged HC subject.

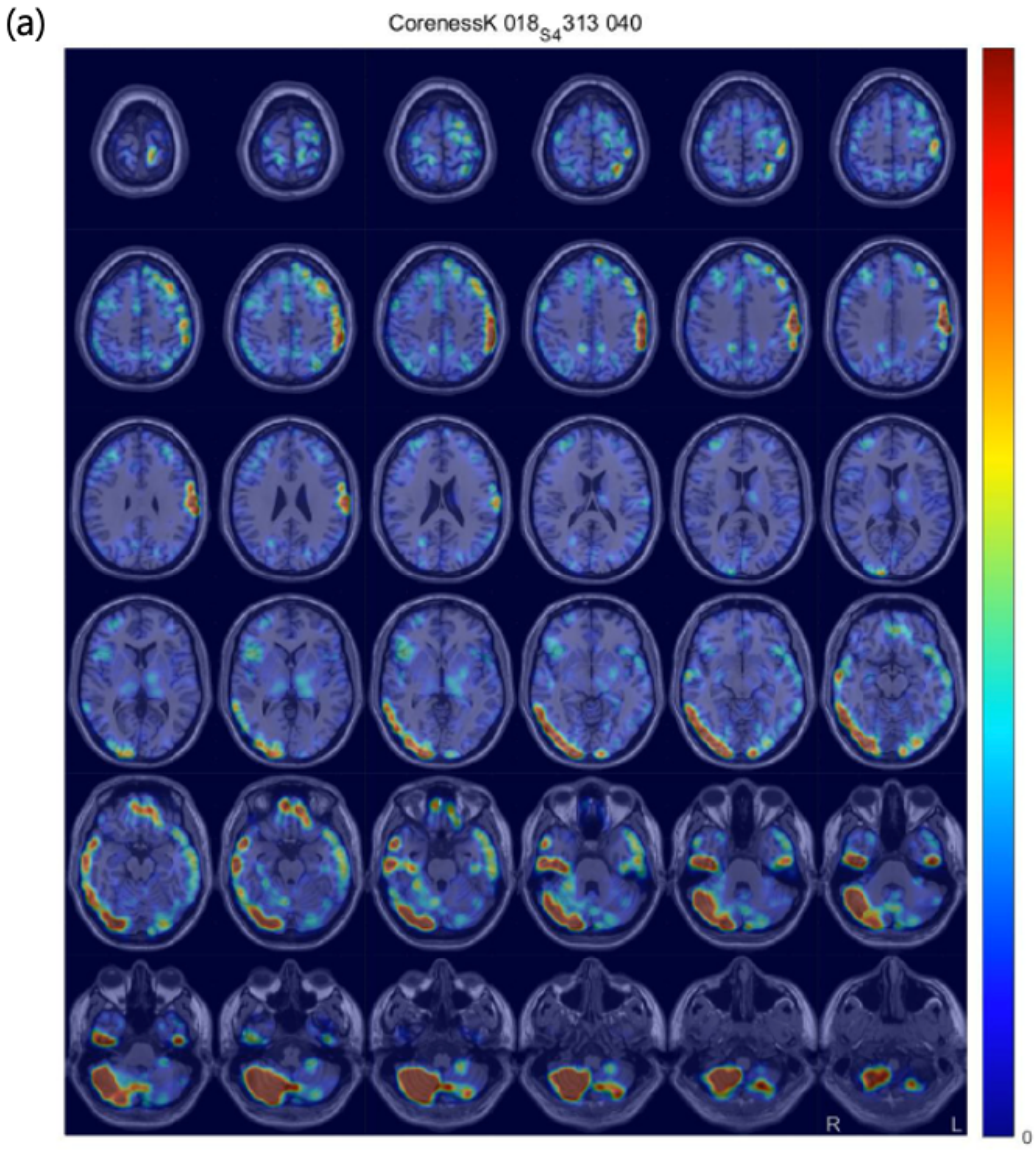

(b)

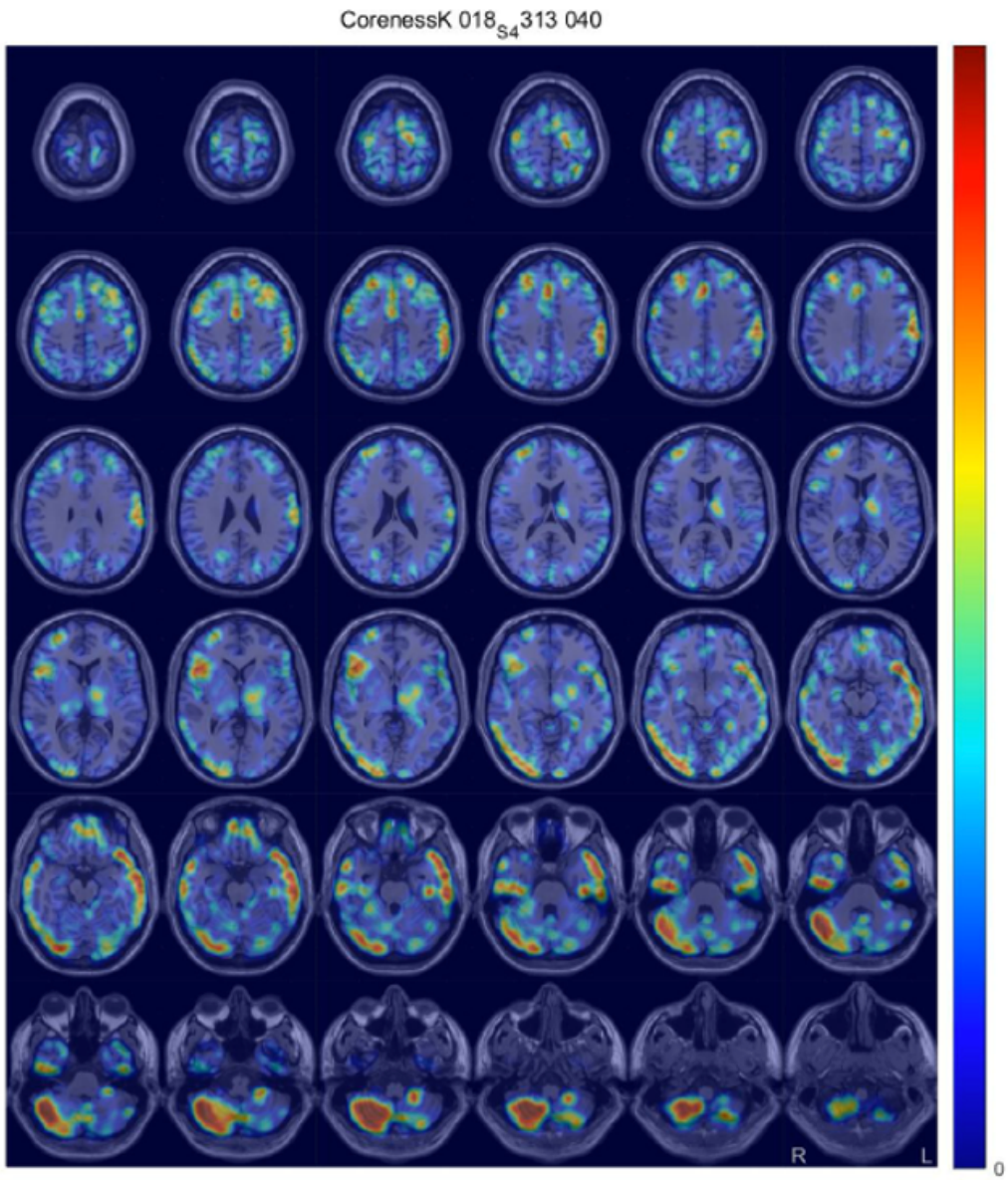

Movie S6. Coreness *k* value maps of summed dynamic positive and negative correlations in young and aged HC subjects: young HC (M/25) (a), aged HC (M/90) (b). Diffuse symmetric, synchronized flow pattern is noted in young HC subject, while relatively asymmetric, unsynchronized flow is displayed in aged HC subject.

(a)

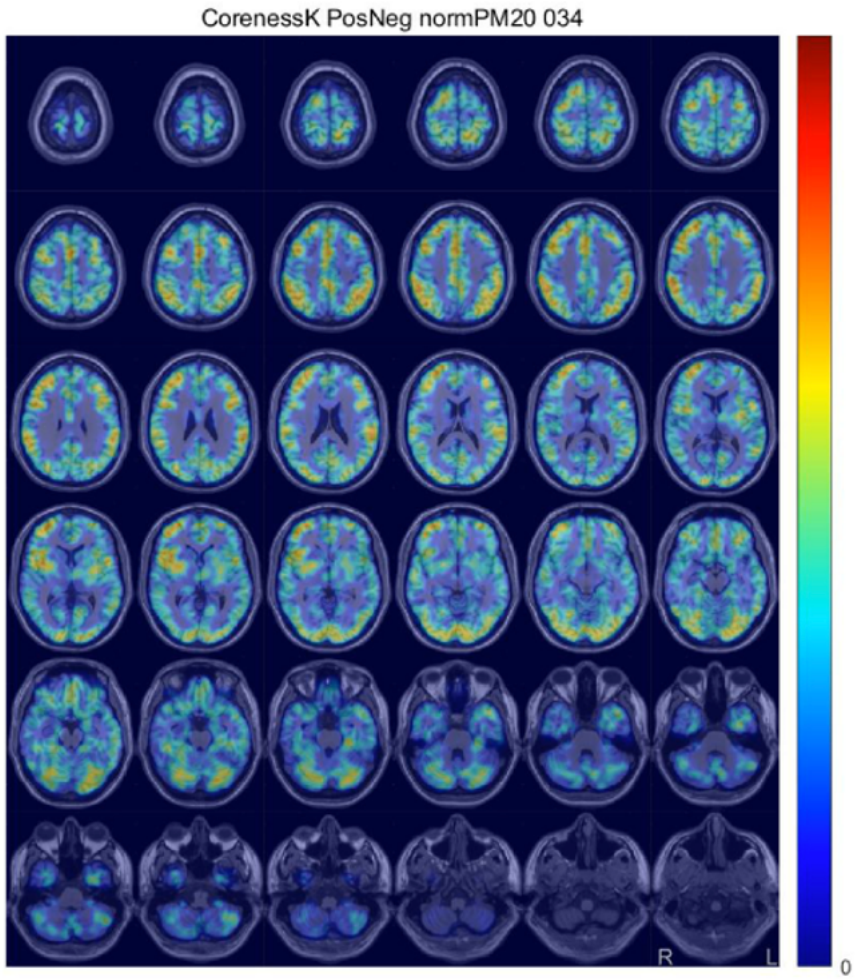

(b)

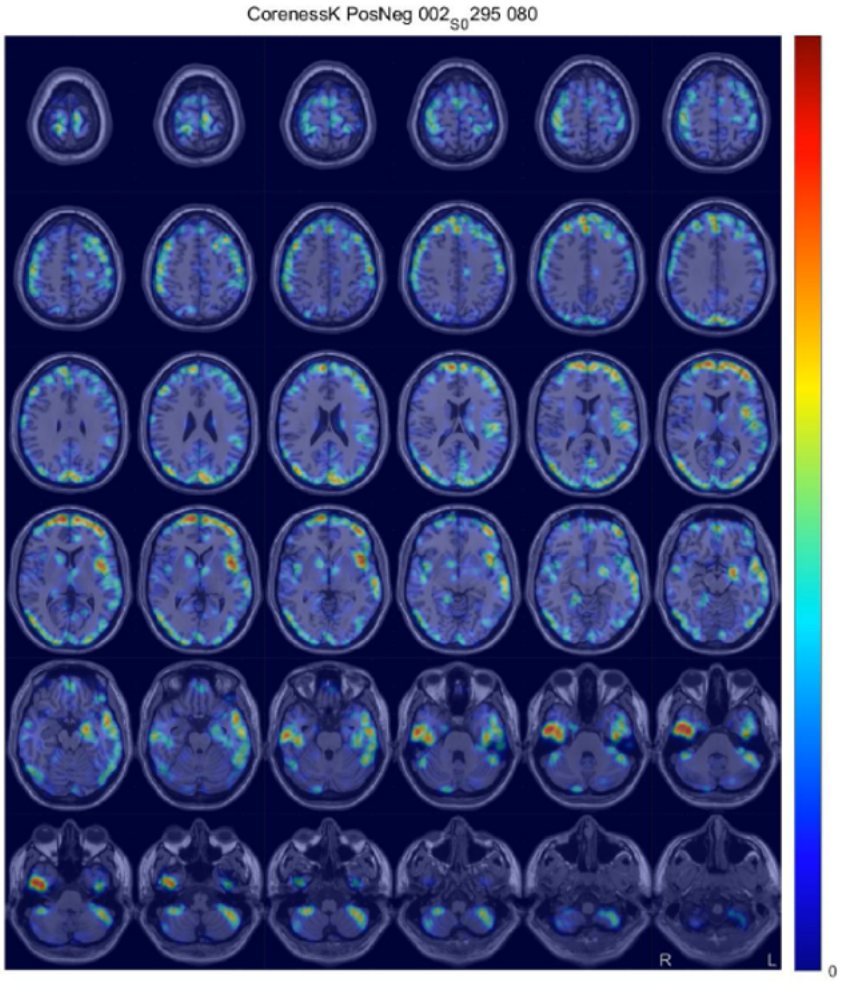

국문 초록

노화에서 뇌기능신경망으로부터 추출한 코어복셀 위계구조의 역동적 변화

김현주

서울대학교

융합과학기술대학원

분자의학 및 바이오제약학과

그동안 뇌 기능을 보다 더 잘 이해하고 분석하기 위해 다양한 분석 방법들이 개발되었다. 이 연구에서는 K코어추출법이라는 방식을 적용하여 휴지기 뇌기능자기공명영상에서 역동적 위계 구조를 복셀 단위에서 밝혀내고자 하였다. 그리고 이 분석방법이 임상분야에서도 적용 가능한지 알아보고자 노화 과정에 적용하여 분석해 보았다.

총 70명을 대상으로 연구가 진행되었는데, 인지 기능이 정상인 대상들을 ADNI에서 32명 그리고 서울대학교에서 38명의 데이터를 받아 분석을 진행하였다. K코어추출법이라는 방법은 복셀 단위로 분석하는 방법으로, 뇌에서 복셀의 위계 구조를 밝혀내기 위해 사용하였다. K코어추출법으로 구한 K최상위코어값, K코어값의 시간에 따른 변화를 히스토그램, 깃발 플롯, 뇌 그림 등의 다양한 방법으로 시각화하였다. 추출된 복셀은 독립요소 분석법을 적용하여 기능적으로 뇌의 어느 요소에 해당하는지 확인하였다. 이러한 분석은 정적, 동적 연구에 사용되었고 또한 양성, 음성 상관 연구에도 사용되었다. K코어값은 뇌 T1 자기공명영상에 얹어서 뇌 내의 분포에 관해서도 분석을 진행하였다.

복셀의 역동적 위계 구조는 시간에 따라 변화하는 K최상위코어값과 K코어값을 동영상으로 만든 히스토그램, 깃발 플롯, 뇌 그림 등으로 시각화하였는데 각 개인의 동적인 뇌 기능 변화가 그림으로 잘 표현되었다. 이러한 동적인 기능적 연결성은 정적인 기능적 연결성에는 담기지 못한 시간에 따른 뇌 기능의 변화에 대한 정보가 담겨 있었다. 또한, 시간에 따른 역동적 변화는 양성, 음성 상관에 따라서 다르게 나타나 신경계 네트워크에 따라 그 변화도 다르게 나타남을 보였다. K코어값 분포도에서는 뇌에서 K코어값의 분포가 나이가 든 군에서 비대칭적으로 나타나는 것을 발견할 수 있었는데, 이는 노화가 진행됨에 따라 악화되는 경향이 있었다. K코어값 분포도에서 발견한 비대칭적 분포는 비대칭 척도를 이용하여 정량화하였다. 그 결과, 젊은 정상군과 나이가 든 정상군에서 차이가 있다는 것을 확인할 수 있었고 그 차이는 정적인 기능적 연결성보다는 동적인 기능적 연결성에서 더 뚜렷하게 나타나는 것을 볼 수 있었다. 또한, 나이가 들어감에 따라 모든 영역에서 정적, 동적인 K코어값 모두 감소하였는데 이는 노화가 진행되면서 뇌의 기능적 연결성이 떨어지는 것을 나타낸다고 볼 수 있다.

K코어추출법으로 복셀 단위로 동적인 기능적 연결성을 분석하였을 때 뇌의 역동적인 위계 구조를 밝혀냈고 이는 시간에 따라 변화하는 각 개인의 뇌 기능을 잘 반영하였다. 정적 기능적 연결성에는 담지 못하는 시간에 따른 정보를 담는다는 점에서 개인의 뇌 기능을 연구할 때 역동적 기능적 연결성을 연구하는 것이 더 적합하다고 볼 수 있다. 이러한 K코어추출법으로 뇌 기능의 역동적인 위계 구조를 밝혀내고, 노화에 적용해서 분석한 것처럼 앞으로 임상에서 다른 분야에도 적용하여 뇌 기능을 연구하는 데에 활용할 수 있을 것으로 기대된다.